CZECH TECHNICAL UNIVERSITY

FACULTY OF MECHANICAL ENGINEERING

MASTER'S THESIS

2022

ANEŽKA

VIMROVÁ

MASTER'S THESIS ASSIGNMENT

I. Personal and study details

Student's name: **Vimrová Anežka** Personal ID number: **459146**

Faculty / Institute: **Faculty of Mechanical Engineering**

Department / Institute: **Department of Automotive, Combustion Engine and Railway Engineering**

Study program: **Master of Automotive Engineering**

Branch of study: **Advanced Powertrains**

II. Master's thesis details

Master's thesis title in English:

Sampling train for a portable air-liquid interface exposure chamber

Master's thesis title in Czech:

Vzorkovací trať pro přenosný toxikologický inkubátor

Guidelines:

Toxicological incubators, allowing for exposure of experimental cell cultures at air-liquid interface, are increasingly used to examine the effects of engine exhaust and other complex mixtures containing nanoparticles, on human health. In this thesis, the sampling train for a portable exposure chamber is to be examined in terms of particle losses, particle deposition rates and possibilities for further reduction of size and mass of the device. Losses of particles in the rotating disc diluter, membrane humidifiers and other parts of the sampling systems, and, if possible, particle deposition rates in the cell cultures, are to be examined during suitable laboratory experiments. Possibilities of a more compact setup are to be examined. Active participation in experiments and cooperation with the Institute of Experimental Medicine of the Czech Academy of Sciences is expected. Details of the assignement will be finalized based on the evolution of the experiments.

Bibliography / sources:

ROSSNER JR, Pavel, CERVENA, Tereza, VOJTISEK-LOM, Michal. In vitro exposure to complete engine emissions–a mini-review. Toxicology, 2021, 152953. (A review paper containing references to relevant additional sources.)

Name and workplace of master's thesis supervisor:

prof. Michal Vojtíšek, M.S., Ph.D., Department of Automotive, Combustion Engine and Railway Engineering, FME

Name and workplace of second master's thesis supervisor or consultant:

Date of master's thesis assignment: **05.11.2021** Deadline for master's thesis submission: **05.01.2022**

Assignment valid until: _____

prof. Michal Vojtíšek, M.S., Ph.D. Supervisor's signature	doc. Ing. Oldřich Vítek, Ph.D. Head of department's signature	prof. Ing. Michael Valášek, DrSc. Dean's signature

III. Assignment receipt

The student acknowledges that the master's thesis is an individual work. The student must produce her thesis without the assistance of others, with the exception of provided consultations. Within the master's thesis, the author must state the names of consultants and include a list of references.

15.11.2021
Date of assignment receipt

Student's signature

Annotation

Author:	Anežka Vimrová
Name of the master's thesis:	Sampling train for a portable air-liquid interface exposure chamber
Academic year:	2021/2022
Department:	12120 Department of Automotive, Combustion Engine and Railway Engineering
Supervisor:	prof. Michal Vojtíšek, M.S., Ph.D.
Bibliography:	
number of pages:	71
number of figures:	59
number of tables:	8
number of attachments:	4

Keywords:

Air-liquid interface, Toxicological incubator, Particulate matter, Engine exhaust emissions, Engine exhaust analysis, Engine exhaust particle sizer, Particle generator, Losses in sampling train

Abstract

Engine exhaust emissions rank among substances possibly carcinogenic and toxic to humans. Models of human lung air-liquid interface are used to simulate the effect of exposure to engine exhaust and other mixtures containing nanoparticles. This master's thesis describes the mechanism of how engine exhaust emissions are formed and their composition and analyses nanoparticle losses in the sampling train for a portable air-liquid interface exposure chamber.

“I declare that this master’s thesis is my own and was created entirely to pursue master’s degree in Automotive Engineering at Faculty of Mechanical Engineering at Czech Technical University. This thesis has not been used for any other degree. I wrote the thesis by myself with using listed sources of information.”

Date

…….

Anežka Vimrová

Acknowledgement

First and foremost, I would like to thank prof. Michal Vojtíšek, M.S., Ph.D. for his guidance and valuable advice during the process of writing this thesis. I would like to also thank Mgr. Tereza Červená, doc. Ing. Martin Pechout, Ph.D. and Ing. Vít Beránek, Ph.D.for their help with the thesis itself as well as experiments.

Finally, I would like to give my thanks to my family for their never-ending support during years of my studying and giving advice when needed.

Table of contents

1. Abbreviations and symbols

Abbreviation	Meaning
PM	Particulate matter
ALI	Air-liquid interface
RDD	Rotating disc diluter
CVS	Constant volume sample
HC	Hydrocarbons
VOC	Volatile organic compounds
SI	Spark ignition
CI	Compression ignition
EGR	Exhaust gas recirculation
DPF	Diesel particulate filter
EEPS	Engine exhaust particle sizer
SMPS	Scanning mobility particle sizer
CPC	Condensation particle counter
DMA	Differential Mobility Analyzer
DR	Dilution ratio
WHTC	World Harmonized Transient Cycle
WLTC	World Harmonized Light Vehicle Cycle

Symbol	SI Unit	Meaning
ρ_{air}	[kg/m3]	density of air at 0°C
λ	[-]	relative air-fuel ratio
p	[atm]	pressure with unit of standard atmosphere
d	[nm]	diameter in nanometers
dN	[#/cm^3]	particle concentration
ϕ	[%]	relative humidity
m	[g/m^3]	density of water vapor in the air at relative humidity
M	[g/m^3]	density of water vapor in fully saturated air

2. Introduction

Ambient air pollution is one of the main factors leading to premature death. Particulate matter (PM) is responsible for a larger number of attributable deaths that alcohol use and equivalent number as high cholesterol and obesity. [1] Worldwide PM contributed to 4.1 million deaths, including deaths from lung cancer, respiratory infections, and chronic lung disease. But outdoor pollution is not the only risk. People using solid fuels for cooking, heating etc. are exposed to "household air indoor" pollution. This indoor pollution was ranked 8th in risk factors in premature death. [1] PM is not the only factor of indoor or outdoor air pollution. Nitrogen oxides (NOx), a part of outdoor pollution, causes approximately 78 thousand premature deaths in Europe. [2] [3]

Due to the particle size the PM is one of the main concerns for population health. Since the primary particle size varies around 10 nm and their aggregates size around 10-100 nm, [2] it can easily penetrate deep into the lungs. Fine particles can penetrate alveoli and interfere with gas exchange between lung and blood. [4] PM often consist of carbon, sulfates, and nitrogen compounds, but their surface chemical composition varies. [5]

Diesel engine exhaust is a mixture of particulate and gaseous components. [3] Both phases can contain carcinogens. [2] [3] It was classified by International Agency for Research and Cancer as a carcinogen to humans (Group 1). Same study classifies gasoline exhaust as possible carcinogen (Group 2B). [6] With introduction of advanced aftertreatment, such as oxidation catalyst, particle etc. the toxicity of diesel exhaust decreases. [2]

The biological impact of air pollutions was studied for approximately fifty years. For these studies, *in vitro* (using various cell models) and *in vivo* (using laboratory animals) tests were used. Animal models (mouse, rat dog, non-human primates) were widely used for inhalation toxicology. Disadvantage of animal tests are differences in the anatomy, physiology and breathing patters between animals and humans. [7] For examining the effects on humans who suffers from respiratory disease (asthma, chronic obstructive pulmonary disease, or pulmonary fibrosis), animal experiments provide data with high failure rates. This is because animal and human models of these diseases are not fully equivalent. [7] The most reliable information on health effect of air pollution is provided by tests on human organism. Unfortunately, these tests are expensive, time consuming as well as limited by ethical reasons [4].

The most advanced method was of cell exposure to pollutants is air-liquid interface (ALI). [4] Unlike other methods of delivering the sample to cell cultures (bubbling through the medium, cell exposed on collagen gels or microporous membranes), the ALI method since it provides similar response in lower sample doses. This is caused by smaller losses in the culture medium. The ALI method is used to cell exposure to a various aerosolized samples such as cigarette some, environmental chemicals, engine exhaust or respiratory viruses and bacteria. [3] [4] [8]

Toxicological incubators are used to simulate the conditions of lung exposure to the engine exhaust and other complex mixtures containing nanoparticles. The cell exposure *in vitro* is linked to the conditions of temperature 37 °C, relative humidity around 85-95 % and concentration of CO_2 around 5 % [2] [3] [4], these conditions simulate the environment of human lungs. Toxicological incubators are used to maintain the temperature, membrane humidifiers or other methods maintain the humidity. Dilution tunnels are used to ensure a constant volume sample (CVS) [2], [3] [4], [8]. To examine the influence of engine exhaust and PM on the cell cultures in real time, a portable toxicological incubator is needed.

In this master's thesis the composition of engine exhaust, the mechanism of formation of engine emission and the sampling train for cell exposure to vehicular exhaust and to PM is reviewed. Losses in the membrane humidifier and the rotating disc diluter (RDD) are evaluated. More compact setup of the membrane humidifier is discussed as well as the possibility of using the RDD instead of the dilution tunnel to obtain the CVS in portable toxicological incubator design.

3. Thesis goals

- Perform experiments for cell *in vitro* exposure to exhaust gases and other complex mixtures with nanoparticles
- Analyze the data and calculate losses in rotating disc diluter and membrane humidifier
- Analyze more compact setup for portable toxicological incubator

4. Engine exhaust emission

Internal combustion engine emits a cocktail of various gasses and particles. These gasses can be toxic or mutagenic or both. The solid particles can also be toxic or mutagenic, and they can also cause mechanical damage. [9] [10]

The products of ideal combustion of HC fuel are CO_2 and H_2O, which make approximately 20 % of exhaust gas [11]. During non-ideal oxidation of H and C from the fuel the products are CO, H_2, PM and hydrocarbons (HC). N_2 is the main component of the exhaust volume wise, when using air as oxidizer. This can be seen in Figure 1. O_2 can also be present when operating the engine in so high air excess, that not all oxygen was used for oxidation of the fuel. In high temperatures various nitrogen oxides NO_X are present. Various organic gases (HC or volatile organic compounds VOC) are also part of exhaust gases. PM includes solid (non-volatile) materials predominantly elemental carbon (black soot). It also includes ash, wear particles and mineral dust ingested by the engine. Semi-volatile compounds, mostly organic compounds originate from incomplete fuel combustion and combustion of engine lubricating oil. [10] [12] [11]

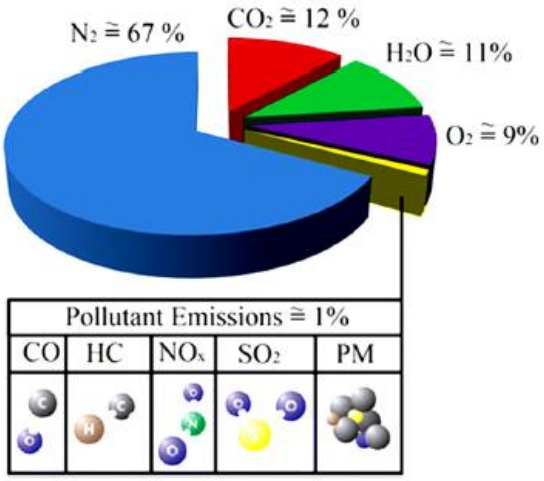

Figure 1: Typical volumetric composition of CI engine exhaust gas [11]

4.1. Analysis of individual component of engine exhaust and its effect on living organism and environment

4.1.1. Carbon monoxide (CO)

CO is a flammable gas without color, taste, or odor. Its density is 1.250 kg/m^3 at 0°C which is slightly less than air (ρ_{air}=1.2754 kg/m^3). It is the simplest molecule of the oxo carbon family, it consists of one carbon atom and one oxygen atom. [9] [13]

In larger concentrations, CO causes poisoning. The CO molecule has stronger chemical bond with hemoglobin than oxygen. When CO creates bond with the hemoglobin in red blood cells, carboxyhemoglobin is created. This means that the red blood cells cannot carry oxygen. This bond is reversible in high concentration of O_2. The symptoms of CO poisoning are dull headache, weakness, dizziness, nausea and in higher concentration loss of consciousness and spasms. The highest risks are for fetuses, because the fetal red blood cells take up CO more readily than adult blood cells. Another high-risk group are children due to their higher breathing frequency. Consequences of exposure to CO depends on concentration and duration of exposure. This dependency is shown in Figure 2. [9] [12] [13] [14] [15] [16]

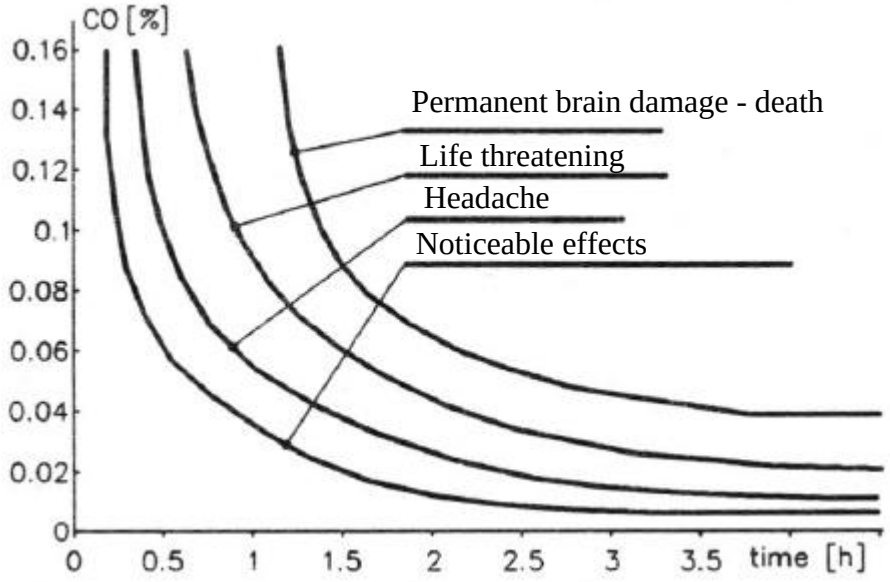

Figure 2: Effects of CO on human organism depending on time and concentration [12]

4.1.2. Carbon dioxide (CO_2)

CO_2 is an acidic colorless gas with a density of 1.977 kg/m^3. CO_2 molecules consist of a carbon atom covalently double bonded to two oxygen atoms. Its sharp acidic odor only appears in high concentration. [17]

Its presence in exhaust gasses is a sign of good engine operation. CO_2 itself is not toxic, but it is one of the greenhouse gases and its atmosphere concentration is linked to climate change. Around 60 % of produced CO_2 is contributing to global warming, the rest (approximately 40 %) [11] is eliminated by plants in photosynthesis processes and dissolved into surface water, which leads to dropping pH of the oceans. [9] [11] [18] [19]

4.1.3. Hydrocarbon (HC)

Even though HC consists only of C and H atoms it is a wide group of organic chemical compounds. Firstly, the carbon atoms create bonds with each other and then the hydrogen atoms join in many different configurations. Based on structure, the HC can be divided into two categories, the aliphatic and aromatic HC. The aliphatic HC are divided according to the types of bonds they contain. Alkanes have only single bonds, alkenes have C=C double bond and alkynes have C≡C triple bond. Aromatic HC consists of a benzene ring, those are classified as arenes, or nonbenzenoid aromatic HC. [20]

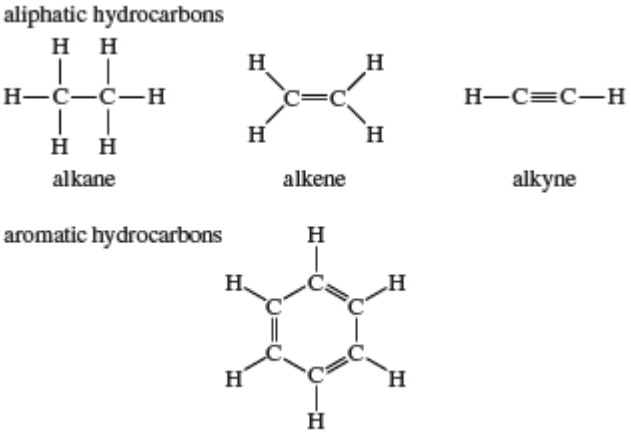

Figure 3: Examples of aliphatic and aromatic hydrocarbons [20]

Mots HC are highly flammable. Some HC are not dangerous at all, and some are mutagenic or toxic. That depends on their potential for oxidant formation. Alkanes and alkenes are not dangerous. Aromatic polycyclic compounds are often carcinogenic. Aldehydes are reactive species and therefore are generally toxic and can irritate mucous membrane. They are also DNA-damaging agents. [9] [21] [22]

4.1.4. Nitric oxides (NOx)

NO is colorless gas. It creates bond with hemoglobin very quickly but is reversible. Naturally, NO is produced during thunderstorms. The intense heating and cooling causes otherwise stable molecules N_2 and O_2 to bond and create NO. Another source of NO is oxidation of fuel nitrogen when air-fuel ratio $\lambda \approx 1$. When $\lambda > 1$ and in atmosphere the NO oxidizes to NO_2. [9]

NO_2 is orange gas with chlorine-like odor. Causes very strong irritation of upper respiratory tract lungs. With HC is a starting point for oxidation reaction which leads to production of ozone by photo-dissociation of NO_2 by sunlight. NO_2 can also form an acid rain when reacting with water, oxygen, and other chemicals in atmosphere. [9] [23]

4.1.5. Sulfur dioxide (SO_2)

SO_2 is colorless toxic gas. Its odor is similar to a just-struck match. It causes strong irritation of mucous membrane and increases risk of infection. It one of the causes of acid rains. [9]

4.1.6. Particulate matter (PM)

PM consists of soot with a reactive surface. This surface can absorb other liquid or solid phase species. PM can be either soluble or insoluble. Some of the absorbed materials can be toxic or mutagenic. The soot particles can also cause mechanical damage and can irritate respiratory tract or eyes. [9]

Soot composes almost half of PM. Particulates consists of liquid organically soluble phase and solid organically insoluble phase. Soluble phase can consist of aldehydes, alkanes, alkenes, or aliphatic HC. Lubricating oil, partially oxidized fuel can also contribute to the soluble part of PM. The structure of PM can be seen in Figure 4 [24]

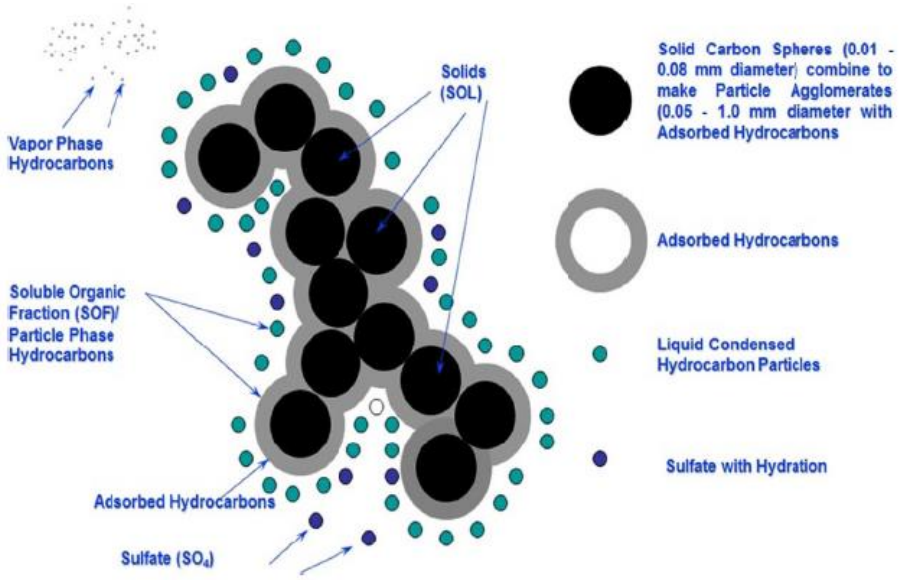

Figure 4: Schematic structure of PM [24]

4.2. Mechanism of formation of emissions in internal combustion engines

The SI engine exhaust gasses contain NO_X, CO, and organic compounds. The oxides of nitrogen are nitric oxide NO and smaller amounts of nitride dioxide NO_2. These oxides are collectively known as NO_X. The organic compounds are unburnt or partially burn hydrocarbons HC. [9] [10]

The amount of NO_X in CI engines is comparable to the SI engine. The HC emission are lower by factor of 5. The HC in the exhaust can condensate and form white smoke when the engine is cold. Some of the HC are the source of CI engine odor. The main danger in CI engine exhaust gasses is the PM. These particles diameter varies from units to hundreds of nm. They consist primarily of soot core with absorbed HC. The PM emissions are significantly lower in the SI engine than in CI engine without a diesel particulate filter (DPF) but are higher than CI engine with a DPF [25]. [9] [10]

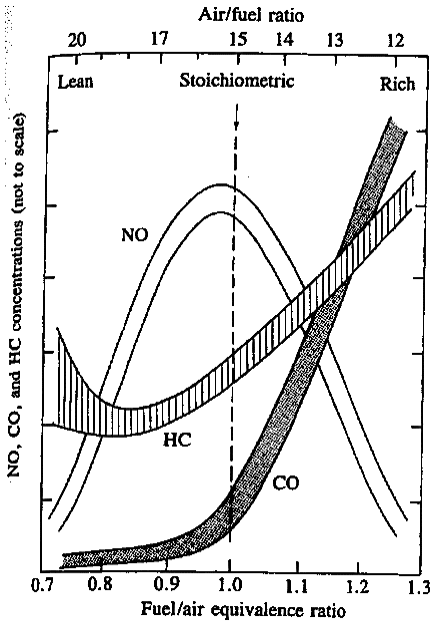

Figure 5:Variation of HC, CO, and NO concentration in SI engine with fuel-air equivalence ratio [10]

4.2.1. Carbon monoxide (CO) formation

CO emissions are influenced by air-fuel ratio. SI engines operates near stoichiometric air-fuel ratio or in fuel rich at full load. Figure 5 shows how rapidly grows volume of CO when closer to stoichiometric region as well as in rich region. The massive increase while leaving stoichiometric ratio is caused by growing adiabatic flame temperature, which leads to thermal decomposition of CO_2 to CO. When moving to richer region, the adiabatic temperature is dropping, hence the thermal decomposition of CO_2 is dropping, but not enough oxygen is present. This leads to CO not being able to oxidize further to CO_2 and concentration of CO is increasing. [10] [26]

The CI engines operates in the lean area, but due to non-homogeneous mixture certain rich local zones are present. This is the cause for higher concentration of CO but due to the fact, that CI engines operates in lean mixtures with air excess, the CO is reduced

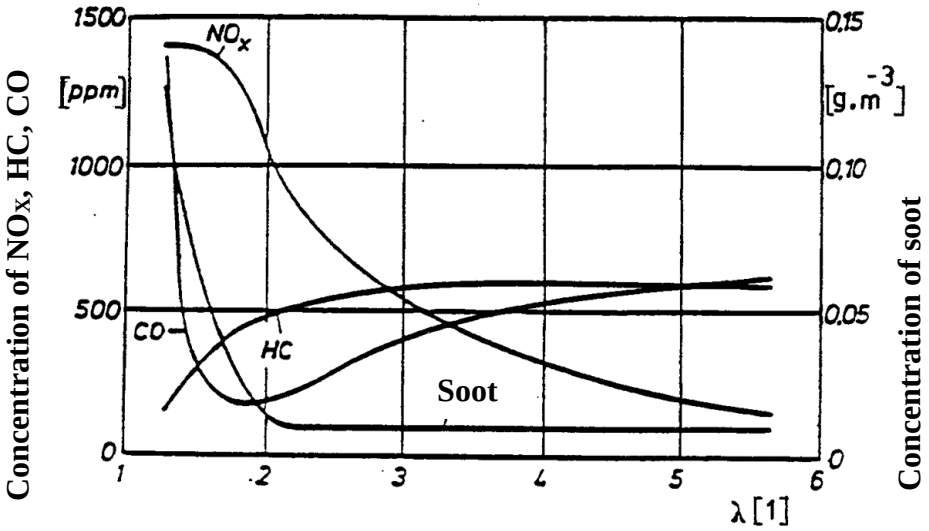

Figure 6: Concentration of emission in CI engines on air-fuel ratio [9]

by oxidation to CO_2. The growing tendency can be seen in Figure 6. This is caused by lower temperature; therefore, the chemistry is too slow and the chemical reaction freezes. The temperature for stopping the reaction is around 1400 K. The CO emissions in CI engines are quite insignificant. [10] [26]

4.2.2. Nitrogen oxides (NO_X) formation

The NO emissions accounts for more than 90 % of total NO_X emissions. The Zeldovich mechanism can be seen in equations (1), (2) and (3)

$$O + N_2 \rightarrow NO + N \quad (1)$$

$$N + O_2 \rightarrow NO + O \quad (2)$$

$$N + OH \rightarrow NO + H \quad (3)$$

Temperature above 1700 K and air excess is needed for these reactions to take place. [9] The high temperature causes splitting N_2 and O_2 into their atomic form. The highest adiabatic flame temperature is reached with slightly richer mixtures, but the lack of oxygen in richer mixture is obstacle for reactions (1), (2) and (3) to happen. Therefore the peak of NO emission formation is moved to slightly leaner mixtures with fuel-air ratio around 0.9.This can be seen in Figure 5, where the NO curve has its peak with fuel-air ratio just below 1. [9] [10] [26] [27] [28]

In CI engines the concentration of NO_X is lower than in SI engines but share of NO emissions is higher. The NO is produced in the flame front. The NO concentration produced by a CI engine is linked to the air-fuel ratio, temperature, and compression ratio.

The CO_2 forms at lower temperature regions (below 1200 K) [28]. It is formed by reaction:

$$NO + HO_2 \rightarrow NO_2 + OH \quad (4)$$

HO_2 is formed in the colder regions of unburned gas, and it reacts with NO formed in the flame front. NO_2 is only exhausted when temperatures are below 1200 K, at temperatures higher than that, it reverts to NO. [9] [26] [27] [28]

NO_X formation can be reduced by Exhaust gas recirculation (EGR). Part of the exhaust gases is returned to the cylinder for mixing with fresh air. The temperature is decreasing with increasing EGR and therefore, the NO_X concentration is also decreasing. [9] [26] [27] [28]

4.2.3. Hydrocarbons (HC) formation

HC or more appropriately called organic emissions are a result of incomplete combustion of the hydrocarbon fuel. Fuel composition is influencing the composition and volume of organic emissions. Fuels that contain high amount of aromatic HC produce higher concentration of reactive HC. [10] [29]

Main source of HC is incomplete combustion of HC fuel. HC will remain only in areas where the temperature is too low for the flame to propagate. Areas like that are crevices in the combustion chamber such as piston top-land volume (the volume between cylinder and piston above top ring), the area within the top-ring groove, which is not occupied by the ring, the valve seat crevices and so on. [9] [26] [29]

Another source of HC can be lubricating oil penetration to the combustion chamber around piston rings or valve lining. The oil stays on the wall and absorbs some of the fuel. The temperature on the wall is too low for the flame propagation due to the quench layer. The piston scrapes HC from the wall to the exhaust port during exhaust stroke. HC that can not be reached by the piston, are removed from the cylinder during early exhaust because of pressure gradient (the pressure in exhaust port is lower than in the combustion chamber). [9] [27] [28] [29]

HC which do not burn in the primary combustion process, they need to survive expansion and exhaust process without oxidizing. Only those will appear in exhaust gasses. HC can oxidize in post combustion when temperatures are around 1200 K. Another oxidation is happening in catalyzing system where the HC oxidizes at temperatures around 700-900 K. [9] [10]

The CI engines are using fuel with higher contain of HC compound with higher boiling points that SI engines. Due to the heavy mixing and oxidizing processes in diesel combustion, there are many factors that contributes to the HC emissions. The procedure of HC formation in CI engines is shown in Figure 7. [10]

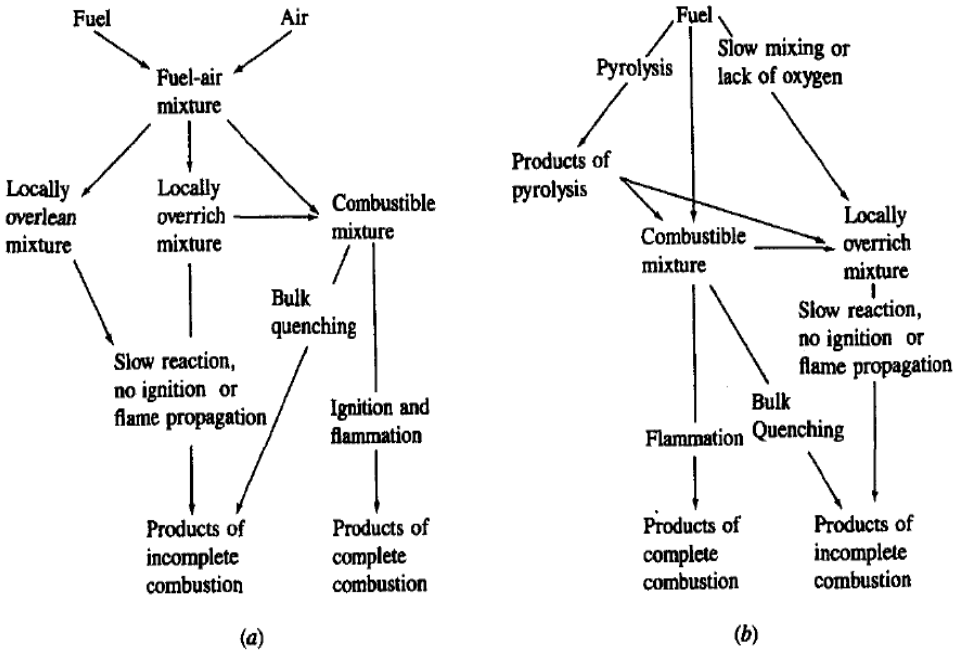

Figure 7: Schematic diagram of HC formation for CI engines, (a) fuel injected during delay period (b) fuel injected while combustion is in progress [10]

Situation when the fuel is injected during the ignition delay can lead to various scenarios. Some of the fuel will form a locally over lean mixture (this will not support any flame propagation or will not auto ignite), some will form locally over rich mixture (combustion of this mixture depends on further mixing with air or already burned gases before expansion), and some will be in combustible range. [10]

If the fuel is injected after the ignition delay period, rapid oxidation of fuel while mixing with air results in complete combustion. When the mixing is too slow, it can result in over rich mixture or quenching, which can lead to incomplete combustion. [10]

The higher air-fuel ratio, the lower the temperature of the flame. The chemical reaction either processes very slowly or can even freeze-up. This leads to increased HC emission in leaner mixtures. This can be seen in Figure 6. The curve of HC is slowly increasing with increasing air-fuel ratio. Generally, the HC emissions are lower in CI engines than in SI engines. [10] [26]

4.2.4. Particulate matter (PM) formation

For SI engines are the main particulate emission organic particles and sulfates. Gasoline contains certain amount of sulfur which is oxidized in the cylinder to sulfur dioxide SO_2. The SO_2 is further oxidized in the catalyst to more dangerous SO_3, which reacts with water resulting in highly corrosive sulfuric acid H_2SO_4. Another cause of particle emission in SI engines is for example un-combusted or partially combusted engine lubricating oil, corrosion particles from the engine parts. SI engines produces lower concentration of PM than CI engines, but CI engines are equipped with a particulate filter and their result emissions are lower (if SI engine does not have the particulate filter as well). [9] [10] [26]

PM in CI engines, including soot, is much bigger problem than in SI engines. Soot forms at extreme local air deficiency where carbon does not have sufficient oxygen to form CO or CO_2. This air deficiency appears locally in CI engines. Soot particulates are form by aggregation of molecules with deficiency of hydrogen. These molecules are chains of carbon atoms. [9] [10]

The process of soot formation depends on pressure, temperature, fuel composition and injection parameters. The oxidation process depends strongly on temperature and pressure. The formation takes place in areas with high temperature and lack of oxygen. The temperatures need to be between 1000 and 2800 K with pressures from 50 to 100 atm. [10] The process consists of six steps. Pyrolysis, nucleation, surface growth, coalescence, agglomeration, and oxidation. [24]

During pyrolysis the fuel undergoes a change on molecular level at high temperature without oxygen. These reactions are generally endothermic and depends on temperature and concentration of air and fuel. Typical products of pyrolysis are for examples polyacetylenes or polycyclic aromatic hydrocarbons. [10] [11] [24]

Particles are formed from gas phase reactants during nucleation. The usual range is around 1.5-2 nm in diameter. These reaction needs temperature around 1300-1600 K. [24] Nucleation phase does not contribute to the total soot mass that much, but it provides big surface area suitable for surface growth. Nucleation forms big number of very small particles. [10]

Surface growth plays a major role in increasing mass of soot. The surface growth rate is larger for smaller particles since they provide bigger surface area. [24]

Next step is coalescence and agglomeration. In this step the particles collide with each other and therefore form a single spheroid. The size of primary particles ranges from 20 to 70 nm, this depends on engine working conditions. After agglomeration the size of particles varies from 100 nm to 2 μm. [9] [10] [24]

When carbon or HC oxidizes it will not be involved in soot formation anymore. This oxidation reaction can happen at any time during the soot formation. Main oxidizing factor is the presence of radicals like OH, O- and O. Oxidation takes place if the temperature is higher than 1300 K. [24] The process of soot formation is shown in Figure 8. [10] [30]

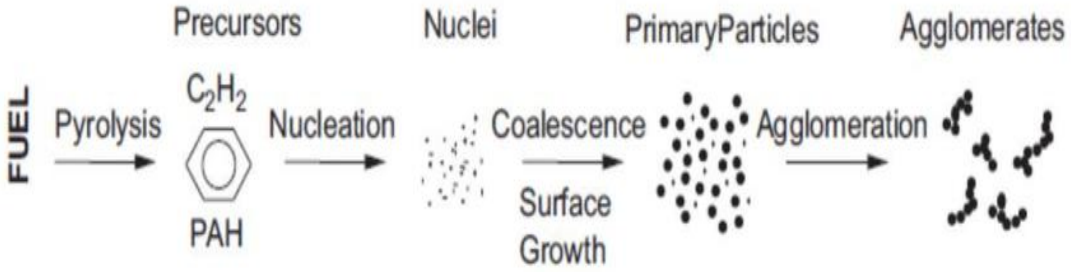

Figure 8: Process of soot formation [30]

Typical scheme of stabilized combustion jet in CI engine can be seen in Figure 9. The yellow area is with high sooth concentration. That is because the temperature is high enough for soot to form and it lacks oxygen, because all radicals needed for oxidation were used around the white dashed line. [10] [24] [30]

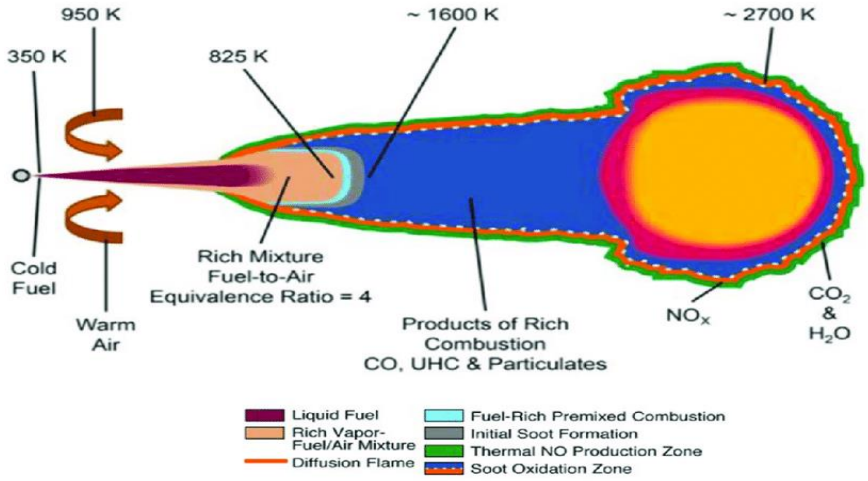

Figure 9: Typical schematic of stabilized fuel jet in CI engine [11]

The combustion particles are not the only ones that are produced. Particles from tires or from brake pads can also be found. Particle concentration from the brake system is similar to the concentration from engine exhaust. [31] Particles can also be generated

from road abrasion. [32] The combustion particles are mainly spherical carbon particles, and they have tendency to aggregate. The mineral particles, for example from road wear,

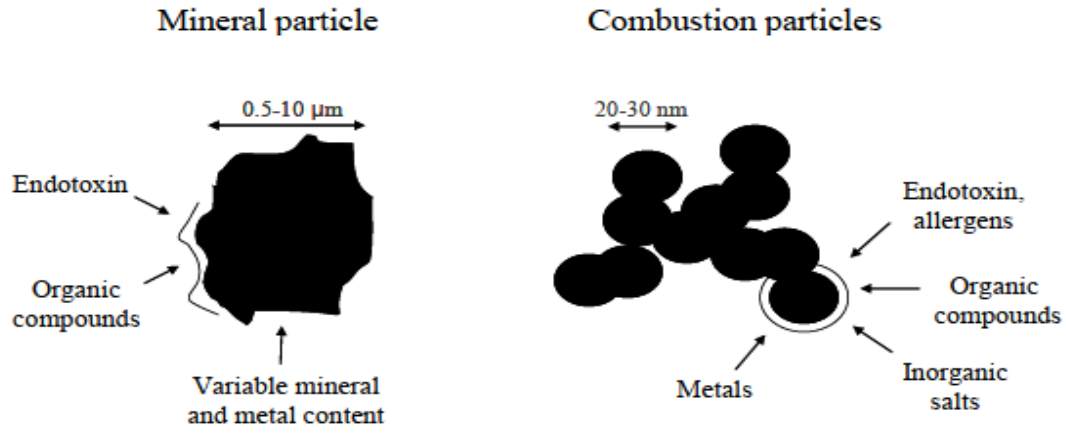

Figure 10: Schematic structure of mineral particle from road abrasion and combustion particles [33]

and are larger. This is shown in Figure 10. In Figure 10 can also be seen larger surface area for of aggregated combustion particles. This leads to bigger potential for adsorption of various possibly dangerous components such as metals, allergens, or toxins. [33]

5. Particle measurements instruments

There are multiple instruments available for measuring concentration and size of particles in aerosol. Both parameters are key factors in determining particle effects on environment and human population. Concentration and composition of sample is needed when using ALI method of cell exposure, or any other method. Particles can be lost in the sampling train, in every crevice, on the wall, a membrane, a flow control, any barrier that is in particles way leads to losses. Therefore, determining the losses is important to know to what concentrations are cell cultures exposed.

5.1. Engine exhaust particle sizer (EEPS), model TSI 3090

The EEPS is using differential electrical mobility classification to sort the particles by their size. The basic principle is to create uniform polarity in the aerosol entering the instrument. With different size particle different electrical potentials are achieved. Those particles then enter the analyzer column near the central rod (Figure 11). Here, they are deflected in radial direction and collected on the outer wall on electrically isolated electrodes. The particle concentration is calculated from electrical current on a series of electrodes. [34]

Inlet aerosol needs to enter a 1 μm cyclone. This is for getting rid of large particles which are out of range. After it the flow enters the charging region where two unipolar diffusion chargers are used for charging. Firstly, a negative charger is used to reduce the number of highly positive particles and then a positive charger to put predictable positive charge on the particles. In the charger fresh air is added in flow of 0.6 liters per minute (lpm) to keep the charger clean. To prevent non uniform charging a flow 2 lpm is removed from the area in the center of charging region. A particle free recirculating sheet flow is added to achieve 49 lpm flow through the column. The flow scheme of EEPS is shown in Figure 12. [34] [35]

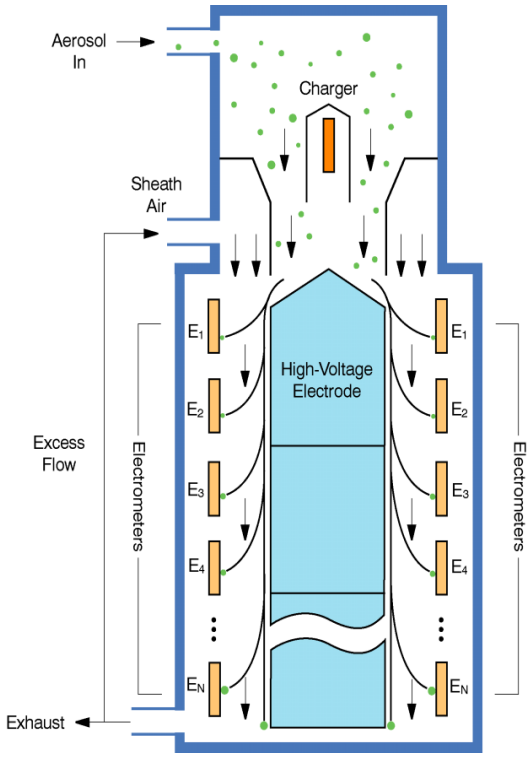

Figure 11: Simple schematic diagram of EEPS model 3090 [35]

The inner cylinder consists of multiple sections with different voltages. The inner rod is split into three parts, and each of them is separately charged into high positive voltage. This causes the particles deflection towards 22 electrodes on the outer wall. These electrodes are electrically isolated by highly insulating plastic. Small particles have higher electrical mobility than larger ones, therefore are deflected toward the electrodes near the top of the column. Large particles are deflected further downstream. [34]

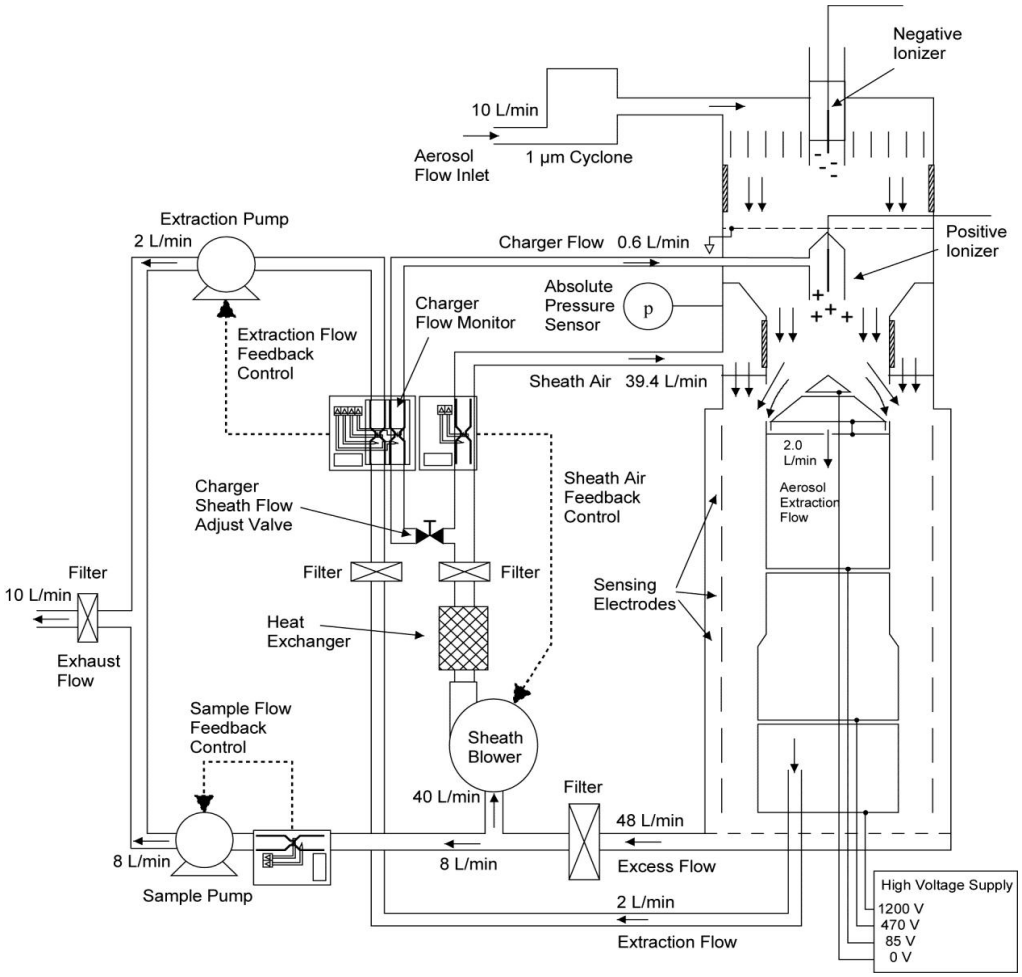

Figure 12: Flow schematic of EEPS [34]

To achieve high time resolution, certain corrections need to be made. There are time delays between detecting smaller particles on the top of the column and detecting larger particles downstream. Particles that do not contact electrodes and only flew pass them can create image charges. Therefore, an inversion algorithm is used for the correction of image charges and time delays. The algorithm converts the 22 currents from electrodes into 32 size channels on output. The output channels are equally distributed between 5.6 nm and 560 nm. [34] [35]

EEPS works between concentration limits given for each output size channel. The lower limit depends on particle size and averaging time. The upper limit depends on the fixed limit of detectable current on each electrometer channel. This limit does not change with averaging time. If the upper limit is exceeded the EEPS is not able to plot the value above it. This affects the shape of distribution. When measuring high concentration close to the upper limit or even exceeding it, cleaning of electrodes is needed to preserve the quality of measurement. [34]

5.2. Scanning mobility particle sizer (SMPS), model TSI 3080

Like EEPS, the SMPS also sorts particles by size. It has three major parts: a bipolar charger (neutralizer), a flow controller, a high voltage controller and a Differential Mobility Analyzer (DMA). The principle is based on monotonic dependency between electrical mobility and particle size. The particles pass through bipolar charger to ensure fixed percentage of particles that carry one unit of charge. By undergoing collisions with bipolar ions, a process known as neutralization or bipolar charging takes place. This achieves equilibrium state with known percentage of particles that carry zero charges, one unit of charges or multiple charges of both polarities. Then the particles enter the DMA and are sorted by their electrical mobility. The electrical mobility is related to particle size and number of charges on the particle. The DMA can be seen in Figure 13. [35] [36]

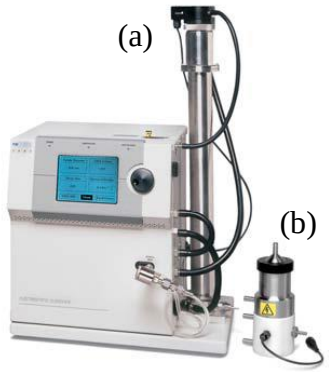

Figure 13: SMPS model 3080, (a) Long DMA (b) nano DMA [36]

The classifier can operate in two modes. First one is overpressure mode during which the CPC dictates the flow rate of polydisperse aerosol. Second one is under-pressure mode, the flow rate is set by the aerosol source entering the classifier. [36]

To process polydisperse aerosol and provide monodisperse output, several subsystems are needed. The major ones are impactor, sheath-air flow controller, neutralizer, high-voltage controller, and DMA. Schematic diagram of the SMPS classifier is shown in Figure 14. [36]

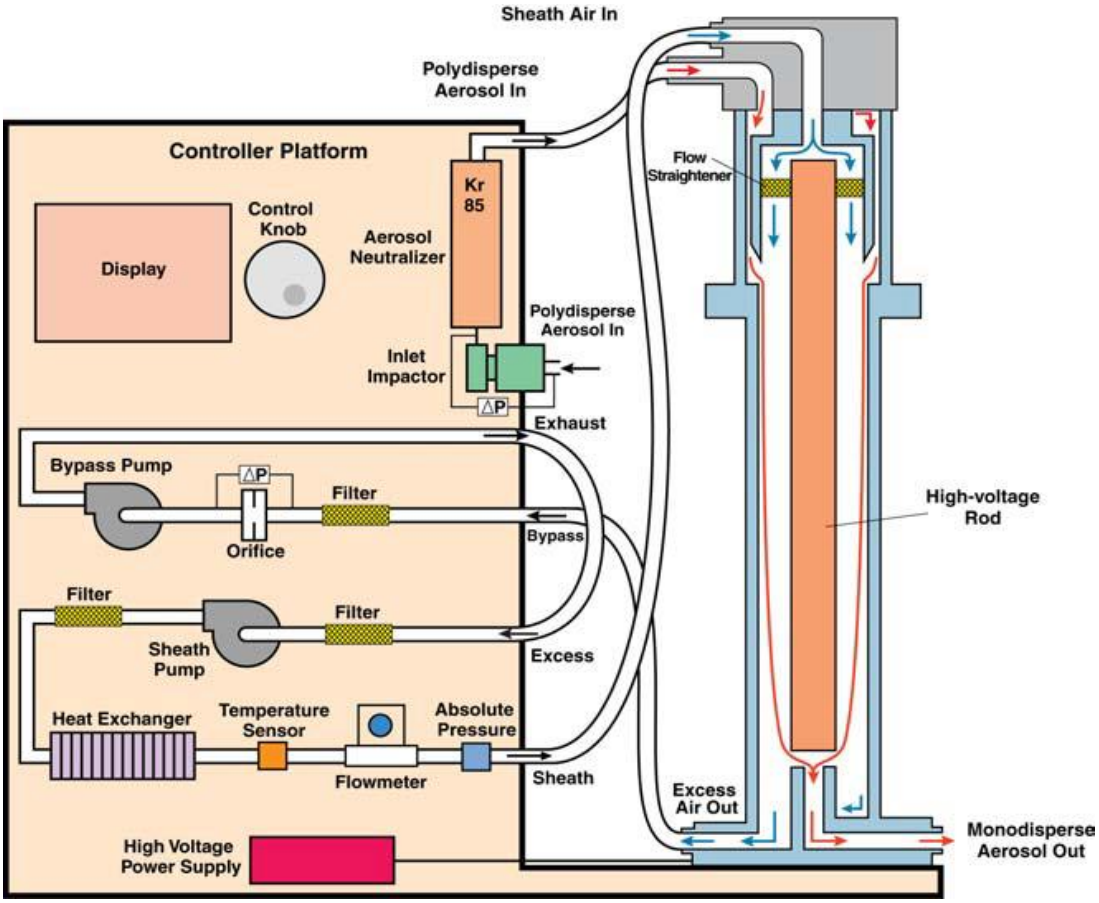

Figure 14: Schematic diagram of SMPS classifier [36]

An impactor is used on the inlet to remove particles that are bigger than known particle size. These large particles contribute to multiplying the charges in aerosol and therefore need to be removed. The impactor consists of a nozzle and an impaction plate (See Figure 15). The plate forces the flow into 90° angle. The particles that are too big and therefore have sufficient inertia, they will not be able to follow the flow and impact on the plate. Smaller particles will follow the streamlines and exit the impactor. [36]

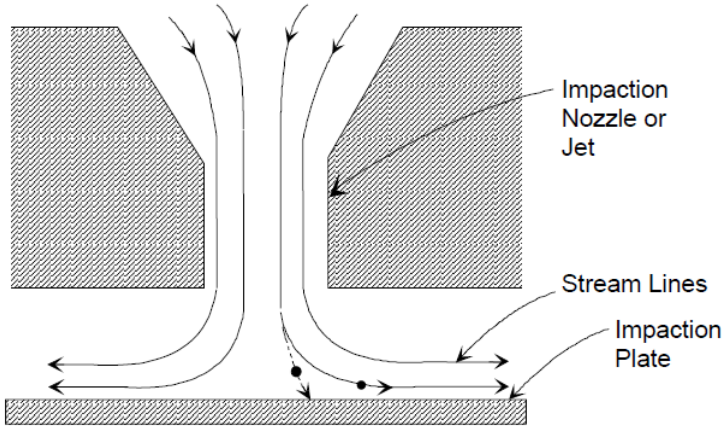

Figure 15: Cross-section of an inertial impactor [36]

A sheath flow controller maintains constant flow through the sheath flow loop. A microprocessor is used to monitor the flow and to control it with a pump. To remove the heat added to the circuit by the pump a heat exchanger is present. [36]

Constant flow through the bypass circuit is maintained by the bypass flow controller. The pressure drops around the orifice and these drops are monitored for controlling the pump. [36]

5.2.1. Long DMA

The long DMA provides range of measurable sizes from 10 nm to 1000 nm. It consists of two electrodes of cylindrical shape made of polished stainless-steel and insulated from each other by spacers. The lower spacer is made of acetyl-plastic. It allows enough high-voltage leakage to prevent static charge build up near the exit slit. This allows better small particles transport. [36]

There are two separate inlets in DMA. One for filtered particle-free sheath flow and one for the polydisperse flow. The sheath flow goes through fine nylon mesh to straighten the flow, the air flows downward in axial direction in the classifier region. The polydisperse flow flows axially as well, but the aerosol flows between two cylinders for evenly distribution. It is then smoothly merged with the sheath flow. Negatively charged particles are removed towards to the outer wall, positively charged particles continue downstream and are attracted to the center in radial direction. Neutral particles are removed with the excess flow. [36]

5.2.2. Nano DMA

The nano DMA provides range from 2 nm to 150 nm. The aerosol enters the short connecting tube. This tube widens to a conical section and forms annular channel. The conical shape allows increased flow of the polydisperse aerosol to the inlet slit. It reduces particles losses by reducing the transport time. The sheath flow enters the nano DMA from the bottom, through the central electrode. After that it is turned backward and flows downwards. The extra air exits the DMA as bypass flow. [36]

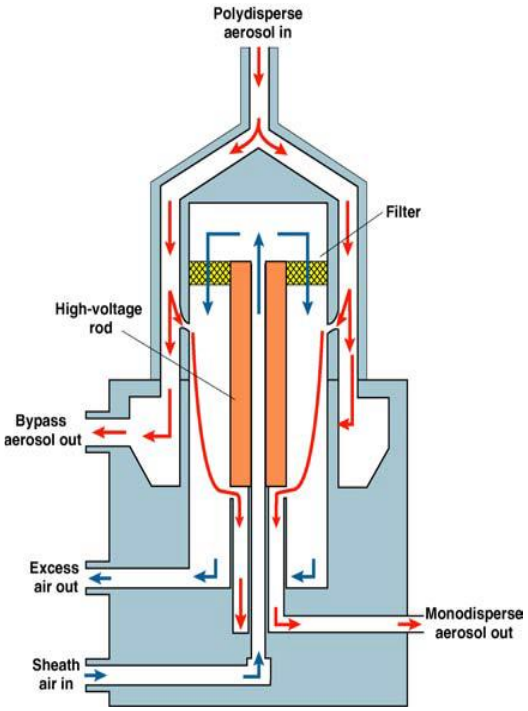

Figure 16: Schematic diagram of the nano DMA [36]

5.3. Condensation particle counter (CPC), model TSI 3022A

The CPC uses principle of condensation of supersaturated vapor on small particles making them bigger and detectable. An aerosol sample is pumped through adjustable inlet. The inlet can be set for high-flow measurement (1.5 lpm) or for low-flow measurement (0.3 lpm). The high-flow setup provides faster response time and minimizes transport losses. The low-flow setup provides flexibility for using with SMPS in serial setup. [37]

1-Butanol is used to saturate the flow. Heated saturator is used for heating the flow to 37 °C. After the sample passes through the saturator it enters a tube cooled to 10 °C serving as a condenser. When exposed to cooler temperature, the butanol condensates onto the particles. This creates easily detectable larger particles (droplets). Optical detector is placed right after the condenser. [37]

The CPC measures in two modes. While concentration is below 10^4 particles per cubic centimeter (#/cc) it measures in single-count mode. The detector detects and counts each single particle. In photometric mode the concentration is measured by light detection. The CPC uses light scattered by all particles at one time and comparing the value to calibration values. This mode measures concentrations up to 10^7 #/cc. [37]

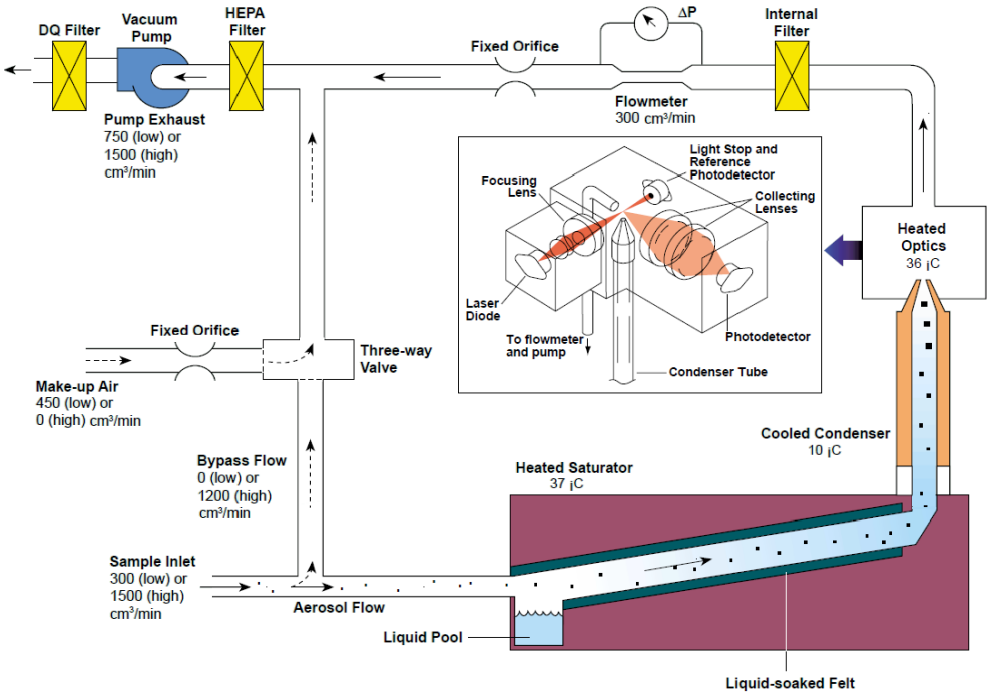

Figure 17: Schematic layout of CPC model 3022A [37]

Relative response curve from [38] can be seen in Figure 18. Particle counting efficiency is decreasing with decreasing particle diameter. Particles with diameter smaller than 7 nm are detected with 50 % efficiency. Particles bigger than 14 nm are detected with more than 80 % efficiency.

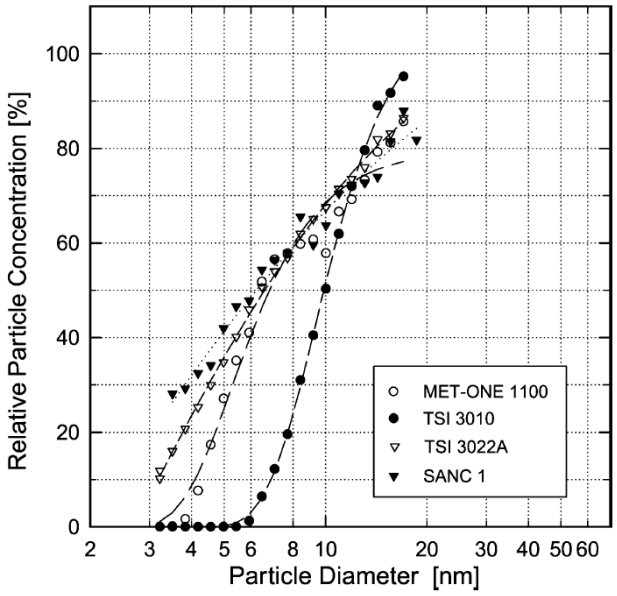

Figure 18: Response characteristic of CPC TSI 3022A for silver particles. Geometric mean particle diameter between 3 nm and 20 nm [38]

5.4. Rotating disc diluter (RDD), type MD-19, Matter Engineering

The RDD is used to dilute the sample to ensure the CVS. It consists of a rotating disk with hemispheric cavities. The disk rotates on a stainless-steel block disposing of two aerosol channels. The hemispherical cavities deliver a defined amount of sample to a fresh airflow. By adjusting the frequency of rotation and volume of cavities, the dilution can vary from 1:15 – 1:3000. The dilution factor depends on the temperature and indicates, how many times higher is the undiluted flow compared to the diluted flow. A dilution factor "15" corresponds to a dilution ratio of 1:15. [39] [40]

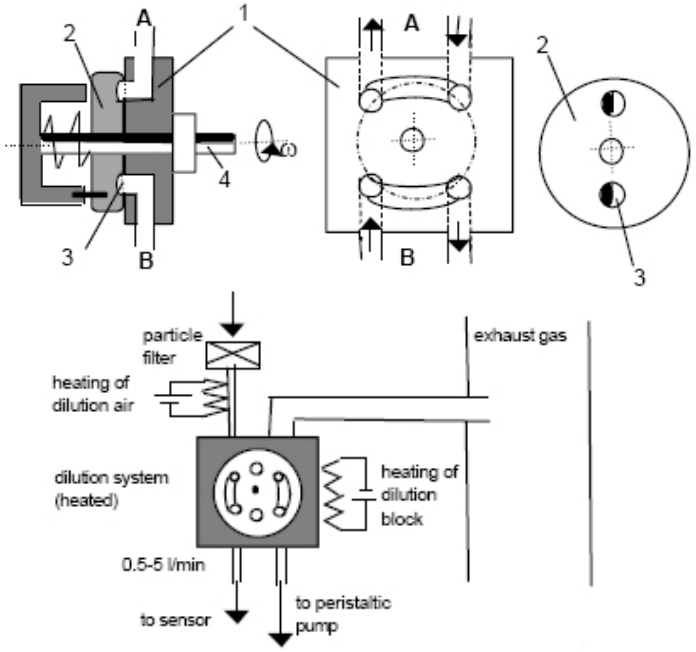

Figure 19: The rotating disc diluter model MD-19. A: undiluted flow, B: fresh air flow, (1) body, (2) rotating disc, (3) cavities [39]

The block and the dilution air are heated to prevent homogenous and heterogenous nucleation of water, sulphuric acids and organic compounds that might be present in the sample. This process is called a hot dilution method, its goal is to prevent nanoparticles to form due to the sampling and dilution and to assure the dilution air flow provides information about particles created by the source of aerosol. [39] [40]

The RDD consists of two main parts, a diluter head (disposing of a heated block and rotating disc) and a control unit. The control unit is connected to the head by two connections: one electrical and one pneumatic, both 3 meters long. So the diluter head is placed closer to the aerosol source. [39] [40]

Losses caused by diffusion take place in the undiluted exhaust and diluted flow tubes. Losses are proportionally dependent on the length of the tube and inversely dependent on the sample flow. Testo manual [40] states, that total losses for 30 nm size particles, with sample flow of 1 lpm and length of the gas tube 3 m are approximately 7 %, under same conditions losses for 10 nm particle are around 10 %. [39] [40]

6. Cell exposure system

ALI system was used for cell exposure. Cell cultures are placed in inserts containing a membrane that allows the deposition of these cultures. Inserts are held by a 128x86 mm 24-well plate. The exposure chamber, see Figure 20, allows the exposition of eight cultures at one time. A stainless-steel distributor is used to divide the flow equally to all cell cultures. The distributor is equipped with eight tubes with a 5 mm outer diameter facing the exposed culture. [2] [3]

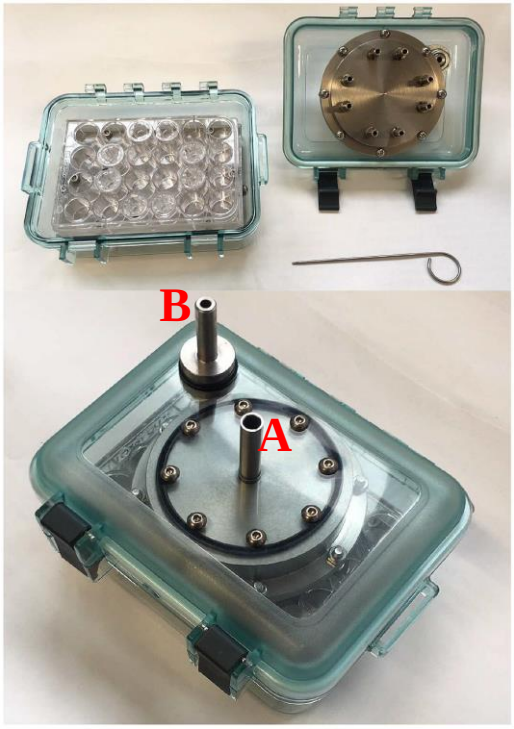

Figure 20: Exposure chamber [2]

The well plate with inserts and the flow distributor are installed in an airtight polycarbonate container. The stainless-steel table is situated on the bottom of the container, and it is adjustable. Sample inflow is in the center of the lid (A in Figure 20) and outlet in the corner (B in Figure 22). The container is designed to a nominal flow of 200 cc per minute, which equals to 25 cc per well. Cell cultures can be prepared in a

controlled area. The container then can be sealed by connecting the inlet and outlet by a tube and transported to an experiment setup.

Exposure chambers (A) are placed in a toxicological incubator (B) maintaining the temperature at 37 °C. Two exposure chambers were used in this study. The first one was used for the sample and was exposed to a diluted exhaust or aerosol with generated nanoparticles. The other one was used as a reference and was exposed to filtered synthetic air. The exposure system can be seen in Figure 21.

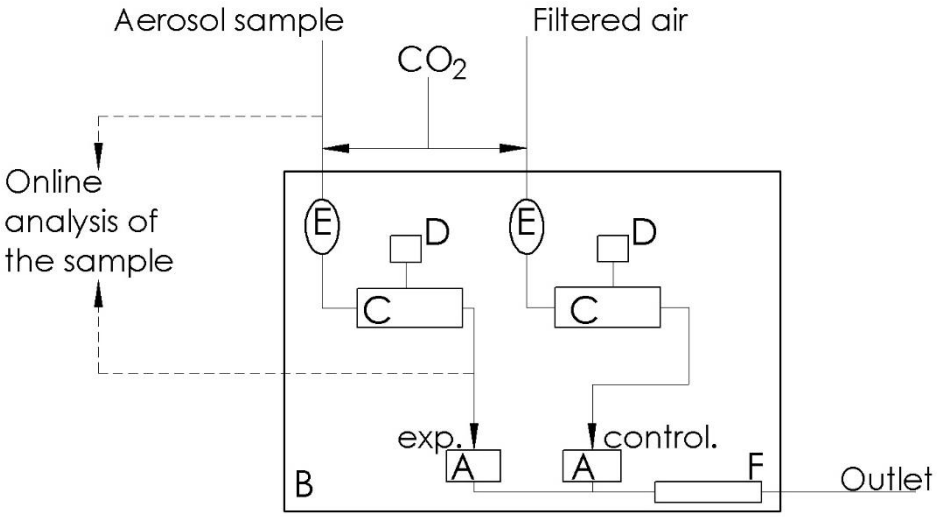

Figure 21: Cell exposure system sampling train; (A) exposure chambers, (B) toxicological incubator, (C) membrane humidifier, (D) deionized water reservoir, € heat exchanger, (F) flow control

On the outlet of the source of the sample, CO_2 is introduced at a concentration around 5 %. CO_2 is introduced to the reference air under the assumption that the reference air does not contain any CO_2. Before the incubator inlet, a flow around 3.3-3.6 lpm is diverted into an online analysis. Flow around 0.5 lpm passes through the incubator wall (B), then through the heat exchanger (E) to be heated up to 37 °C and through a membrane humidifier (C) (PermaPure model no. FC125-240-5MR). Deionized water is supplied from a water reservoir (D) installed on top of the humidifier. The relative humidity needs to be 85-95 % to simulate the human lung environment. On the humidifier outlet a flow of 0.3 lpm is diverted into an online analysis and a flow of 0.2 lpm passes through the exposure chamber. The flow is controlled by rotameters with a needle valve (F) located downstream of the exposure chamber.

A particle generator or a diesel engine were used as a source of sample flow. Those setups are described in the following chapters.

6.1. Experiment with the particle generator (PG)

A particle generator (PG) was used as a stable source of nanoparticles. Particles of 4 materials – Gold, Copper, Iron and Carbon were used to determine losses in the membrane humidifier. This experiment was primarily used to determine the toxicity of the particles. Concentration and size of particles can be varied by adjusting voltage, current and flow of N_2 through the generator.

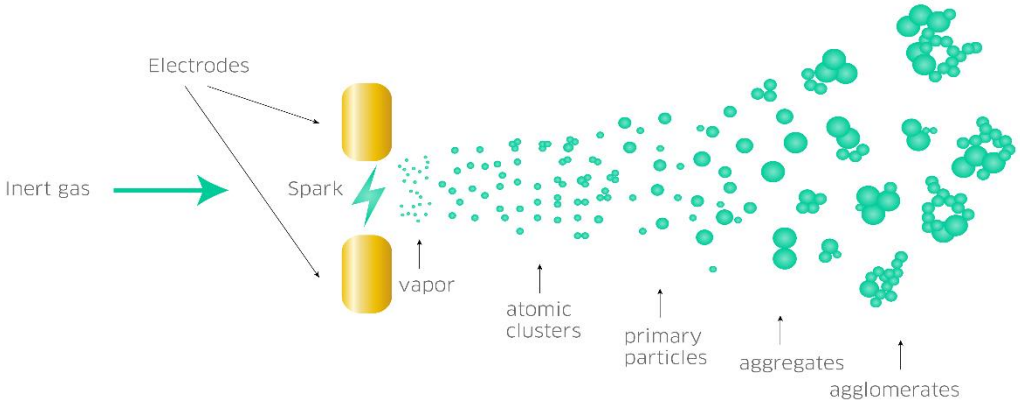

Figure 22: Nanoparticle production by spark ablation [41]

The inert gas serves as a protective atmosphere. It prevents oxidization from happening. By using inert gas N_2 pure metal particles were produced. Particle surface was free from organic contaminants. Particles were generated in the process of spark ablation. Short lasting sparks (1-10 μ) cause strong evaporation of the electrodes. [41] Vapor is carried further downstream with the flow of inert gas and after agglomeration it creates primary particles and later agglomerates. The scheme of nanoparticle production by spark ablation can be seen in Figure 22.

6.1.1. Experimental setup

The schematic experiment setup can be seen in Figure 23. The real pictures in Figure 24 and Figure 25. For sample flow analysis the EEPS (D) and the SMPS (E) in serial connection with the CPC (F) were used. To calculate the losses, the SMPS was used in two setups. In the first setup, during cell exposure, the SMPS (E) was connected serial with the exposure chamber (K), see the dash line in Figure 23. For the second setup, the SMPS (E) was connected right after PG (A). This setup was used for calculation of losses in the membrane humidifier (PermaPure model no. FC125-240-5MR) (G).

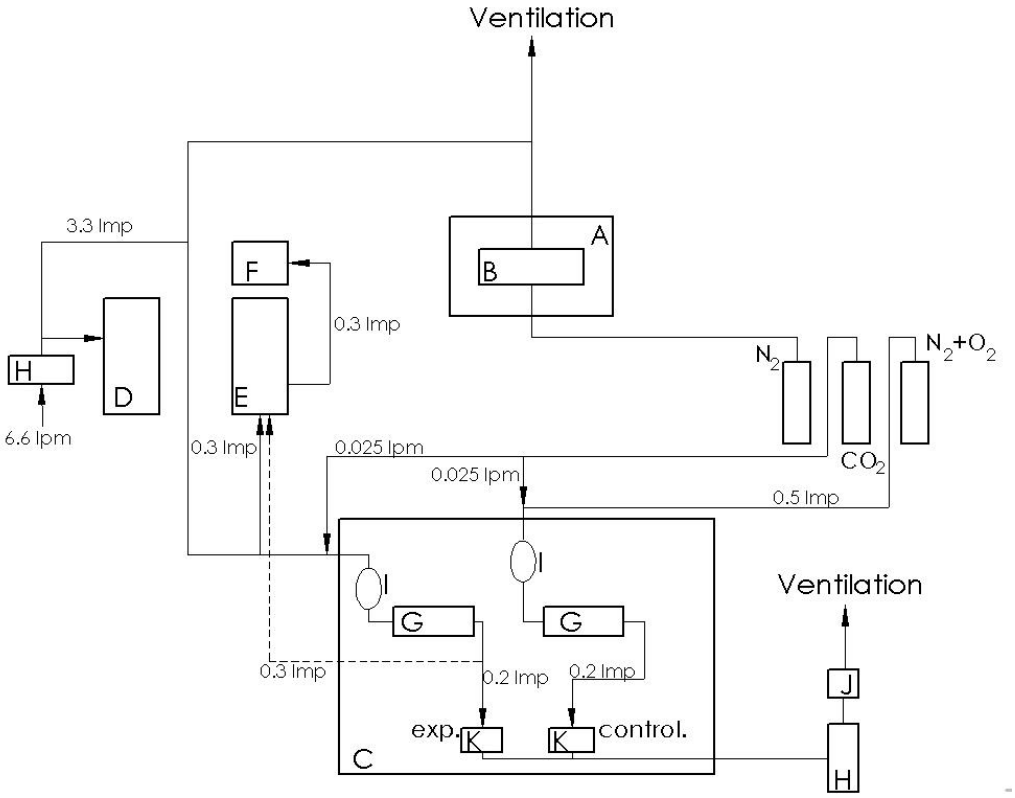

Figure 23: Experimental setup; (A) Body of the PG, (B) Head of the PG, (C) Incubator, (D) EEPS, (D) SMPS, (F) CPC, (G) Membrane humidifier, (H) Hepa-filters, (I) Heat exchangers, (J) Pump, (K) Exposure chambers

The EEPS (TSI, type 3090) was used to measure electrical mobility of the particles and their size distribution at 1 Hz rate. The EEPS (D) was sampling mixture on the PG outlet. The inflow of filtrated air was approximately 6.6 lpm and intake of sample approximately 3.3 lpm.

The SMPS (TSI, type 3080 with 3081 DNA) with CPC (TSI, type 3022A) were used for sampling on the outlet of the membrane humidifier cells to obtain information about concentrations and particle sizes on the cell cultures. The SMPS was running with sheath flow of 3 lpm for gold, iron, and carbon electrodes and with 10 lpm for copper. When measuring smaller particles (d < 14 nm), SMPS concentrations were multiplied by published detection efficiency of CPC (TSI 3022A) for silver particles [38].

Electrode of chosen material was placed in the head of the PG (B). The flow of inert gas N_2 was introduced. Flow rate through the PG varies and depends on the used electrodes. After that the spark was initiated. Before the inlet to the incubator (C) around 3.3-3.6 lpm flow rate is diverted to online particle monitoring (EEPS (D) or EEPS (D) and SMPS (E)).

SMPS is sampling from the outlet of the humidifier parallelly with the exposed exposure chamber (K) (see the dashed line in Figure 23). The flow that continues to the cell samples into exposure chamber (K) is nominally 0.2 lpm. Rotameters with needle

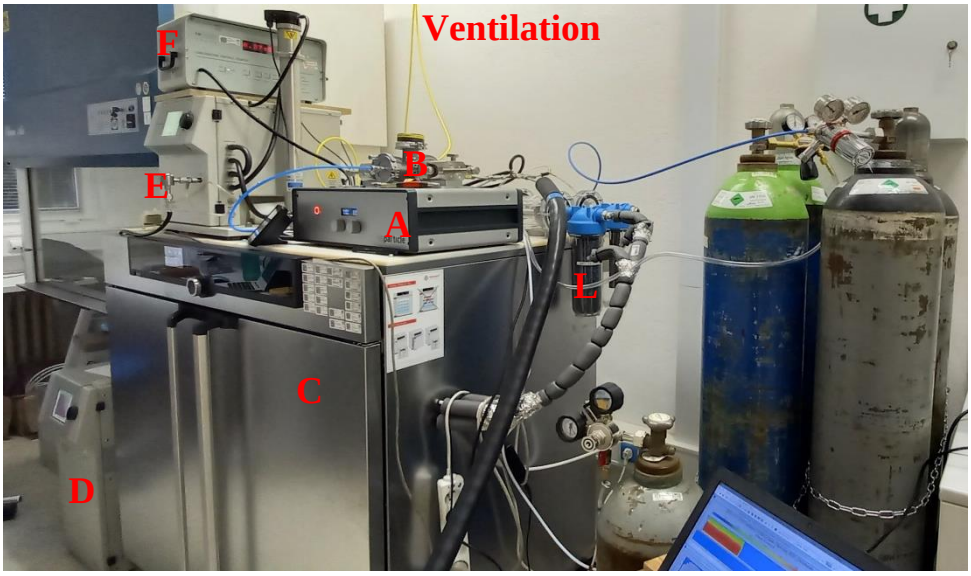

Figure 24: Real experiment setup; (A) Body of the PG, (B) Head of the PG, (C) Incubator, (D) EEPS, (E) SMPS, (F) CPC, (L) Silica gel dryer

valve were used to adjust the flow rates. To simplify the schema, they have not been included there. Can be seen in Figure 25. The pump (J) is used for pumping the CO_2 through the sampling train.

CO_2-enriched synthetic air was introduced to the cellular samples in the reference (control) exposure chamber. On the outlet the flow needs to go through a dryer with silica gel (L). Due to the fact of being almost 100 % humid, the flow needs to be dried before it can leave through ventilation. See Figure 24.

Losses in the membrane humidifier were determined as a difference in total concentration on SMPS between two setups. Results are presented as percentage of lost particles dependent on their size as well as comparison of losses in the membrane humidifier of different materials.

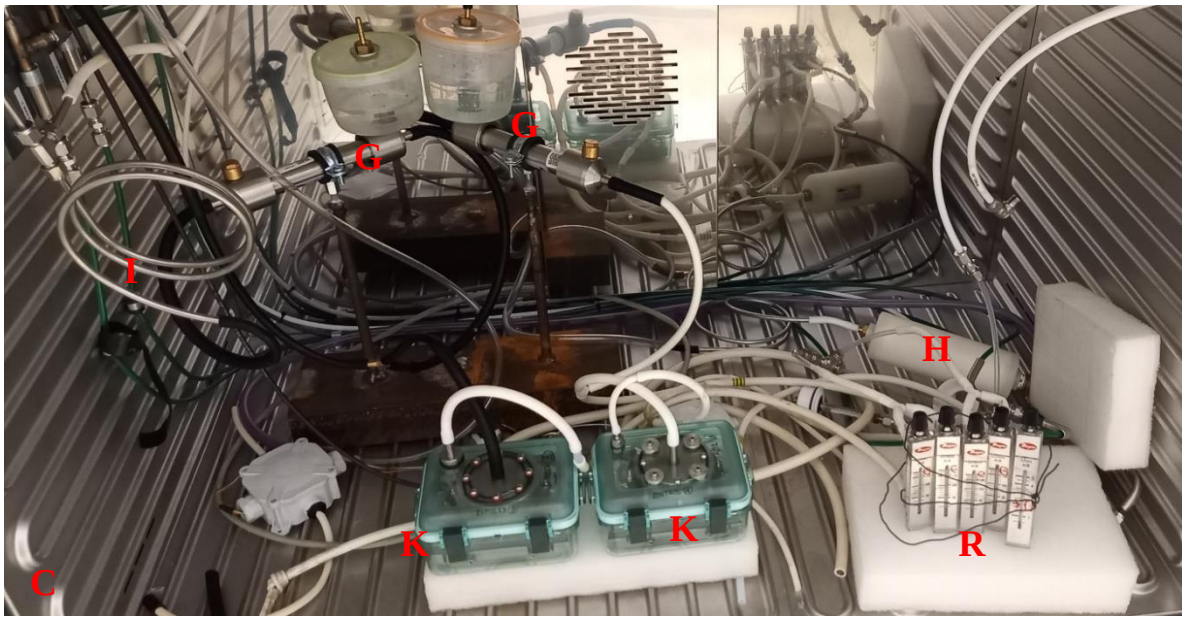

Figure 25: Inside of the Incubator (C); (G) Membrane humidifier, (H) Hepa-filter, (I) Heat exchanger, (K) Exposure chamber, (R) Rotameters

6.2. Experiment with CI engine

The RDD (type MD-19, Matter Engineering, n. 101496, number of disc: 69090/12/01/36) was used to further dilute the sample that was already diluted in dilution tunnel. Sample was taken from a diesel engine (Iveco Tector, 6.6 l) exhaust. Engine was connected to dynamometer (AVL DynoExact 304/8) and run on the World Harmonized Transient Cycle (WHTC).

The sampling train can be seen in Figure 26. The engine was connected to a dilution tunnel to ensure constant volume sample (CVS). The dilution tunnel flow was set to 70 meters per second ($m.s^{-1}$). From the dilution tunnel outlet flow 3.3 lpm was redirected to the EEPS for analysis. When the RDD (D) was connected, the sample first entered the RDD and after that a flow 3.3 lpm was redirected to the EEPS.

The RDD worked with potentiometer set on 2. The dilution ratio (RD) is given as 178.7 for potentiometer value of 1 and 62.0 for potentiometer value of 2.5 (From calibration list dated 17.9.2013). After recalculation by weighted arithmetic mean value, for the potentiometer value of 2, the DR is 78.8. The RDD works with the inflow of 0.5-5 lpm, the EEPS works with inflow of 10 lpm (the EEPS was taking flow around 6.6 lpm of fresh air through hepa-filter). Due to that fact the sample was diluted 2:1 on the inlet of EEPS. Total DR is then 157.6.

The losses on RDD were obtained as a difference between total concentrations on the EEPS when EEPS was sampling on the outlet from the dilution tunnel (dashed line in Figure 26) and when it was sampling on the outlet of the RDD. The above stated calibration ratio was considered.

Cell cultures were placed in the exposure chambers (G) (See Figure 20). One of the exposure chambers was connected to the sample flow and the other one to filtered air flow for reference. CO_2 in concentration around 5 % on the cell cultures was introduced to both chambers. The flow was controlled by rotameters with needle valves placed on outlets of the exposure chambers.

Sample and control flow entered the toxicological incubator (C) which was heated to 37 °C. Flow then went through the heat exchanger to be heated up. The membrane humidifier (PermaPure model no. FC125-240-5MR) was used to create humidity around 85-95 %. Temperature 37 °C, concentration 5 % of CO_2 and high humidity simulates the environment of human lungs.

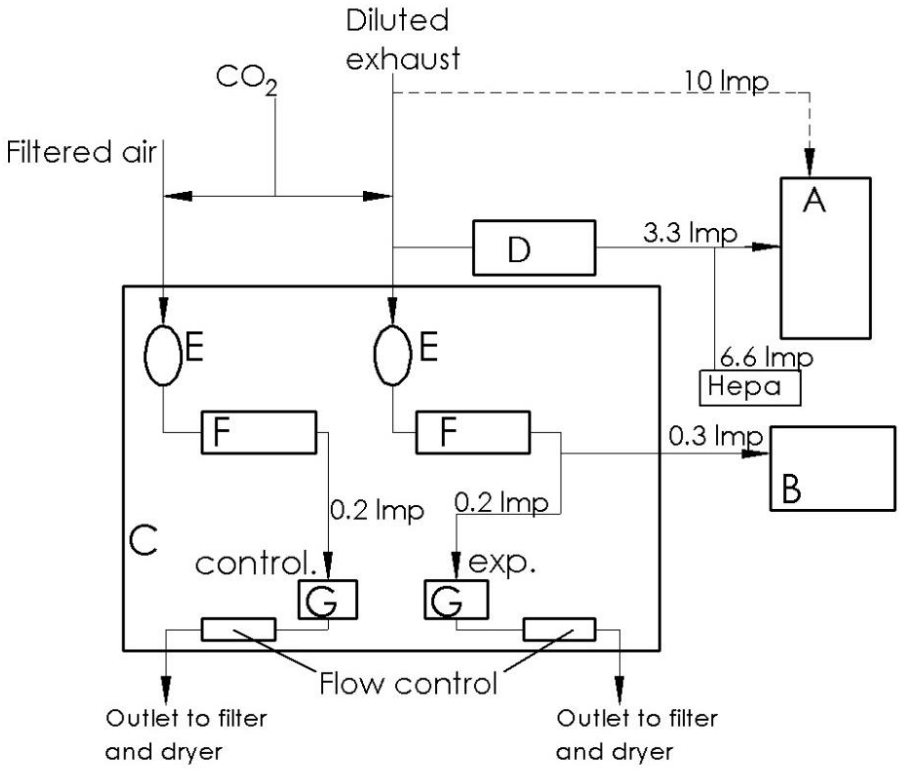

Figure 26:Smpling train; (A) the EEPS, (B) the CPC, (C) the toxicological incubator, (D) the RDD, (E) heat exchanger, (F) the membrane humidifier, (G) the exposure chamber

7. Results

7.1. Losses in the membrane humidifier

The CPC and the SMPS were connected serially The SMPS sorted particles by size and the CPC counted particles. The SMPS provides data in samples, where each sample took 3 minutes to complete the whole spectrum. The sheath flow was set to 3 lpm for Au, C and Fe, for Cu it was set to 10 lpm to try to detect smaller particles. The size range for the sheath flow 3 lpm was from 14.6 nm to 615.3 nm, for the sheath flow 10 lpm the range was 7.37 nm to 289 nm. To achieve better results the SMPS concentrations were multiplied by the detection efficiency of the same CPC model TSI 3022A for silver nanoparticles provided in literature [38]. This response curve can be seen in Figure 18.

Resulting file from the CPC provided particle concentration for each sample. Each of these samples had concentration for each size channel. To plot the concentrations before and after the humidifier a model samples were chosen. By averaging values from these samples, the concentrations can be plotted as a function of the particle diameter. Due to this averaging, concentrations can be plotted as two curves, one for samples before the humidifier and the second one for samples after the humidifier.

The results provided by the EEPS included concentration (#/cc) as a function of time and particle size. For each one of the 32 output size channels a value of concentration as a function of time were calculated by the instrument. To compare these results to results from SMPS and CPC the concentrations needed to be multiplied by 16, which is the number of channels per decade. The channels were equally distributed from 6.04 nm to 523.3 nm. The EEPS also provides data on total concentration.

The resulting file from the EEPS consists of concentrations in each size channel during time of the measurement. The EEPS scans every second. The SMPS scans only every 3 minutes. The values from the EEPS were chosen to match the time of the chosen samples from the SMPS. After determining the time of the SMPS samples the values from the EEPS file were averaged to get a single curve representing the concentrations in the EEPS as a function of the particle diameter.

7.1.1. Gold electrodes

In Figure 27, the average concentrations measured by the SMPS as a function of particle size are plotted. Due to the SMPS limitation in size range, large portion of spectrum is missing, and only last third or so is visible.

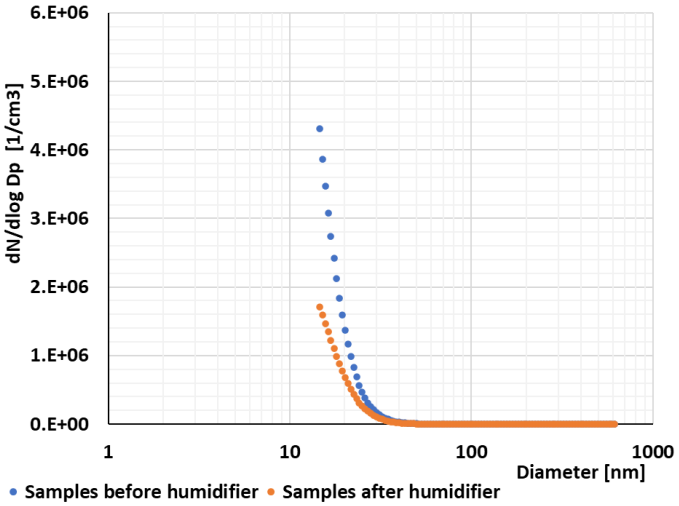

Figure 27: Mean particle size distribution of gold particles before and after humidifier measured by the SMPS. The SMPS was sampling from the PG outlet for "Samples before humidifier", and from the humidifier outlet for "Samples after humidifier"

From the SMPS data on geometrical mean value of particle diameter were obtained. But since the maximum value of the diameter is not in the measurable range, those results are not included. When looking in Figure 32, the geometrical mean value of particle diameter was around 10 nm as measured by the EEPS.

From measured samples on the SMPS representative samples were chosen. Losses for gold particles were determined as a difference between total concentration in samples taken from the humidifier outlet and the PG outlet. The concentration on the membrane humidifier outlet were 56.68 %, 54.10 %, 49.94 %, 55.80 %, 43.33 %, 51.89 %, 43.55 %, 46.65 %, 41.44 %, 43.39 %, 37.03 %, 34.04 %, 40.82 %, 31.15 % and 37.87 % (44.51±7.89 %) lower than on the outlet of the PG. See Table 5. The mean total concentration determined from the EEPS sampling from the PG outlet was determined as 5,71±0,38 million #/cc.

The particle losses also depend on size of the particle. This is shown in Figure 28. For particle diameter 14 nm the losses are 60 %, and then it is declining, and the smallest losses are for particles around 70-80 nm. The biggest losses by percentage are in particle size around 500 nm, but the concentration of these big particles is very small in comparison to particles around 14 nm. The curve is also not stable for larger diameters.

In Figure 29 the comparison of size distribution from the EEPS and SMPS can be seen. The EPPS concentration was multiplied by 16 because of the channel size difference between the EEPS and the SMPS. The EEPS curve peak is around value of 10 nm.

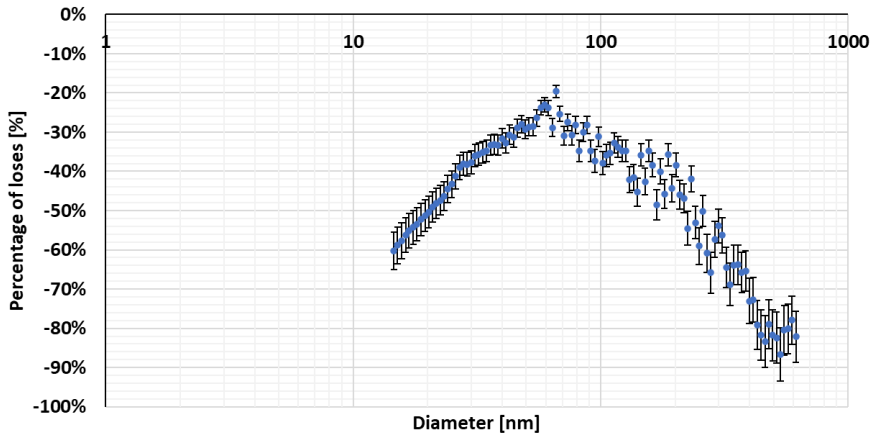

Figure 28: Percentage of losses as a function of particle diameter

For comparison of spectrum of the EEPS and SMPS, the EEPS spectrum was cut to the same size as the SMPS spectrum. Both instruments were sampling on the same spot from the PG outlet. The cut off spectrum ranges from 14 nm to 523 nm. This is shown in Figure 29. The size distribution is very similar.

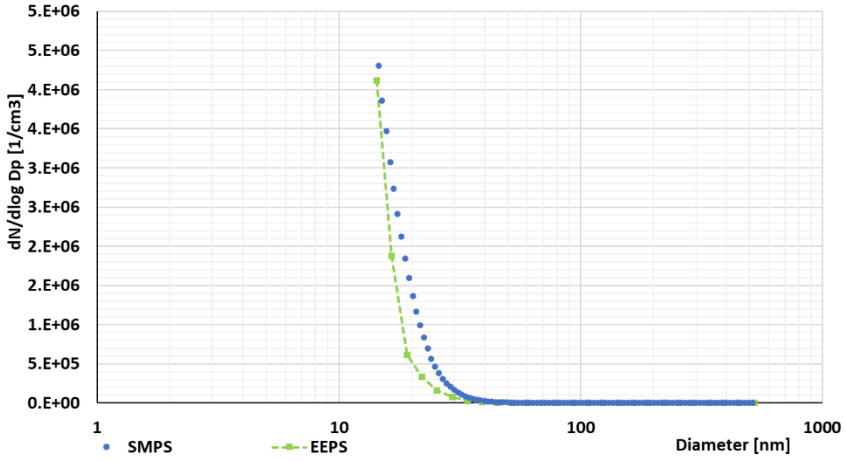

Figure 29: The cut off spectrum of the EEPS in comparison with the SMPS spectrum

7.1.2. Copper electrodes

For copper the sheath flow was set to 10 lpm and therefore corrections are needed, therefore every SMPS curve was multiplied by the response curve in Figure 18. In Figure 30 are shown results for size distribution of Cu particles before and after the humidifier. Concentration of Cu particles from the SMPS before and after the humidifier is on the main y-axis and particle counting efficiency is on secondary y-axis. These concentrations were obtained from the SMPS. The highest concentration is at 12 nm particle size.

The size of particles is shown in Table 1. The geometrical mean value of diameter before the humidifier was found as 13.927±1.331nm. The particle diameter after the humidifier is larger by 5.66 %, nominally 14.715±1.372nm.

	Samples before the humidifier	Samples after the humidifier	Difference [%]
Geo. Mean [nm]	13.927	14.715	5.66
Geo. Std. Dev. [nm]	1.331	1.372	

Table 1:Geometrical mean value of copper particle diameter. Geometric standard deviations represent variance among approximately 4 hours of testing.

Total concentrations on the outlet of the membrane humidifier from the chosen SMPS samples were 68.33 %, 69.56 %, 66.13 % and 68.17 % (68.05±1.42 %) lower than concentrations on the outlet of the PG. See Table 6. The mean total concentration determined from the EEPS sampling from the PG outlet was determined as 2,1±0,47 million #/cc.

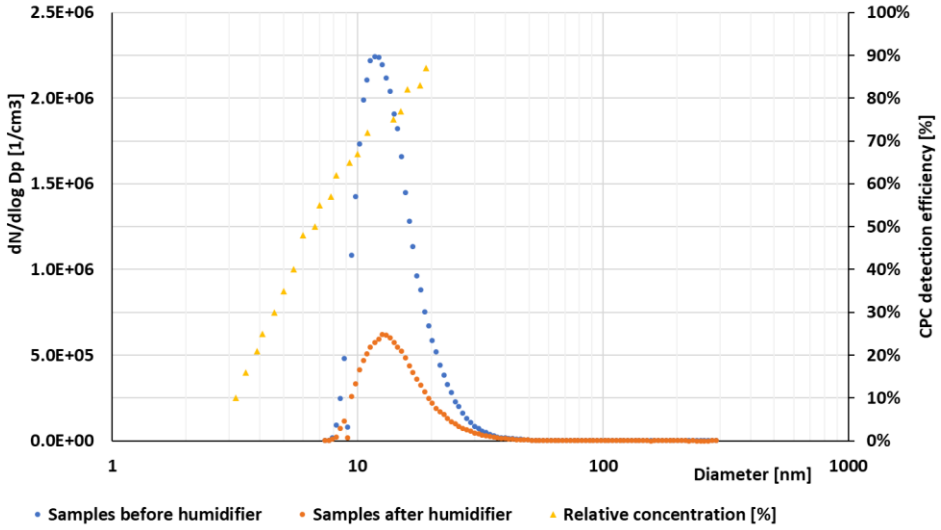

Figure 30: Mean particle size distribution of copper particles before and after the humidifier measured by the SMPS. The SMPS was sampling from the PG outlet for "Samples before humidifier", and from humidifier outlet for "Samples after humidifier". Both curves were multiplied by the response curve from literature [38]

The dependency of particle losses can be seen in Figure 31. Similar trend to Au can be seen in particle diameter from 10 nm to 80 nm. The losses are decreasing in this interval. For particles around 40-90 nm the values vary from losses 40 % to gain 40 %. For large particle with diameter above 100 nm, no stable curve is visible, but the losses are increasing.

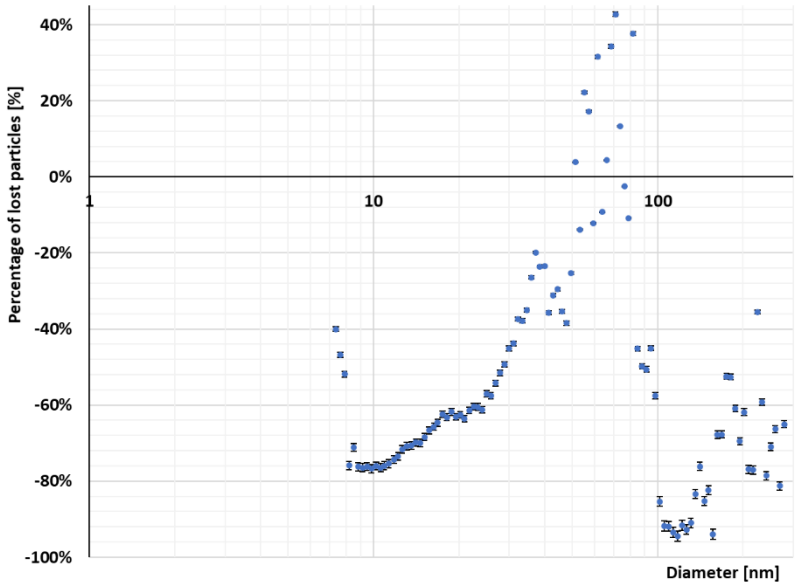

Figure 31: Dependency of Cu particle losses on particle diameter

Comparison of the size distribution from the EEPS and the SMPS is shown in Figure 32. The EEPS curve peak is also around 11-12 nm. The peak concentration measured by the EEPS is around three times larger than the one measured by the SMPS.

To compare both spectra from the EEPS and the SMPS while sampling from the same spot after the PG, the spectrum from the EEPS needed to be cut to match the SMPS spectrum. New range is from 7 nm to 294 nm. See Figure 34.

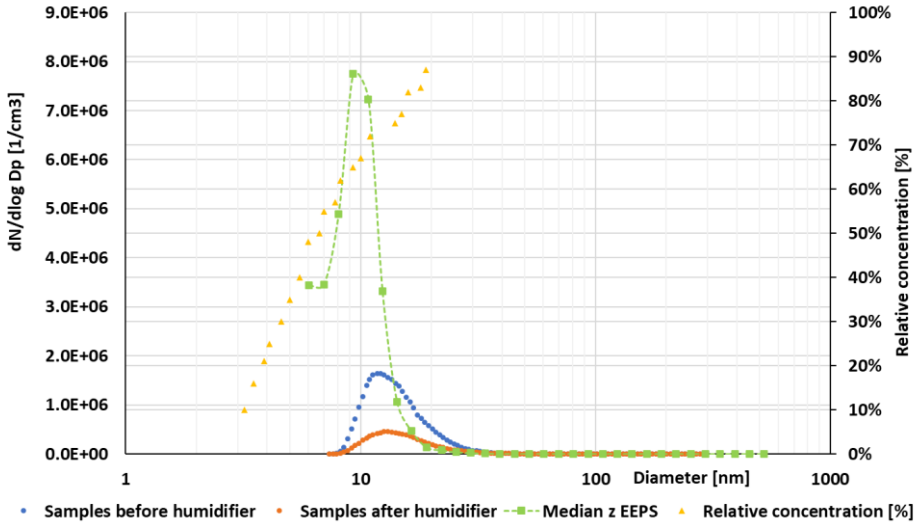

Figure 32: Comparison of mean particle size distribution from EEPS, and SMPS before and after the humidifier. The EEPS were sampling from the PG outlet

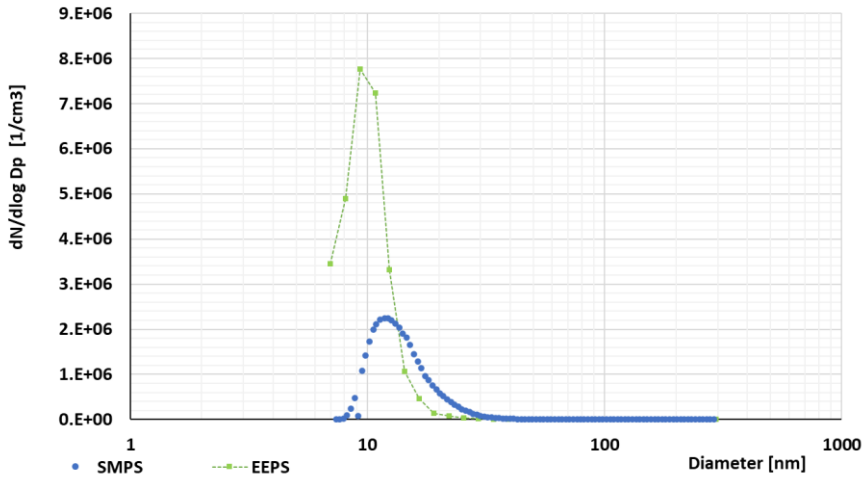

Figure 34: Comparison of size spectra from the EEPS and the SMPS on the same sampling spot, the PG outlet

7.1.3. Iron electrodes

The sheath flow for iron electrodes was set at 3 lpm. This gives range from 14.6 nm to 615 nm. Dashed blue and orange lines in Figure 33 represent the part of spectrum that is missing (out of range). The line A around 20 nm diameters approximately marks where the CPC most probably switched to photometric mode due to the drop in concentration. Line B around 50 nm approximately marks where the CPC switched back to single particle detection mode due to the slight increase in concentration. To smooth out the curve a correction was made.

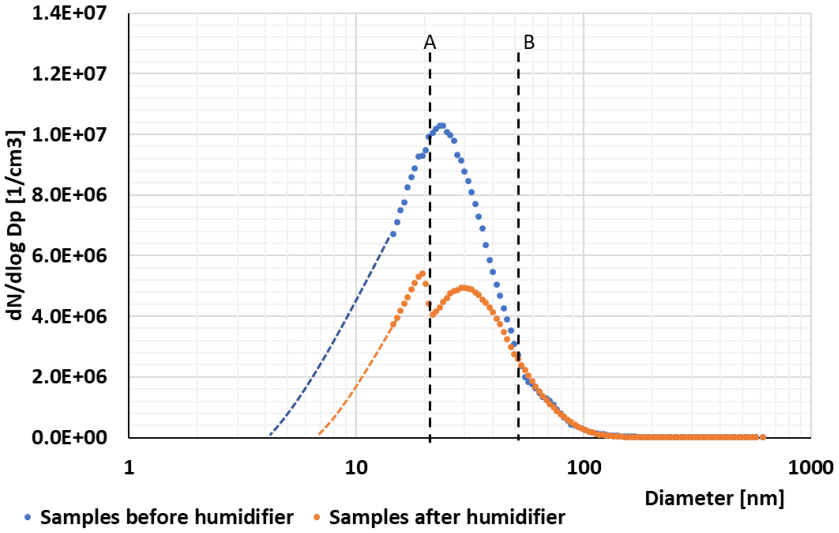

Figure 33: Mean particle size distribution of iron particles before and after humidifier measured by the SMPS. The SMPS was sampling from the PG outlet for samples before humidifier, and from the humidifier outlet for samples after humidifier. Line A – the CPC switched to photometric mode, Line B – the CPC switched to single particle detection mode

Concentration in photometric mode (from 20 nm to 50 nm) was multiplied by an empirical calibration factor 1.4. This factor was obtained by looking at the plots and trying out different values. This correction was made by hand. The smoothed curves are shown in Figure 35.

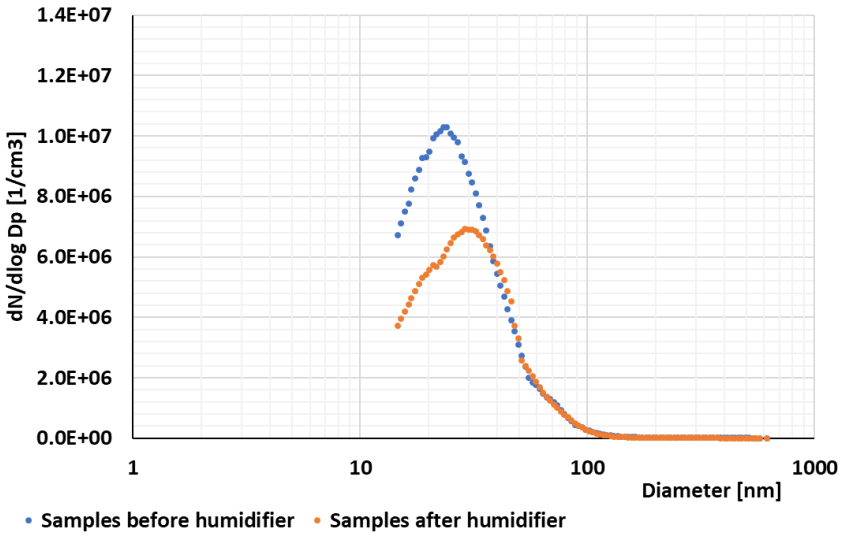

Figure 35: Corrected concentration by multiplying by the empirical calibration factor

The geometrical value of diameter before the humidifier was obtained as 27.269±1.513 nm. The particles after the humidifier are by 9.14 % larger with geometrical value of diameter 29.763±1.578 nm. Total concentration dropped by 43.65 %.

Total concentrations of iron particles before the membrane humidifier were obtained from SMPS samples. Concentrations were 45.29 %, 25.83 %, 39.51 %, 20.59 %, 47.37 %, 41.36 %, 39.10 %, 25.82 % and 45.31 % (36.69±9.96 %) lower than before the humidifier. The mean total concentration measured by the EEPS sampling from the PG outlet was determined as 10,50±1,53 million #/cc.

	Samples before the humidifier	Samples after the humidifier	Difference [%]
Geo. Mean [nm]	27.269	29.763	9.14
Geo. Std. Dev. [nm]	1.513	1.578	

Table 2: Geometrical mean value of iron particle diameter. Geometric standard deviations represent variance among approximately 4 hours of testing.

The losses were plotted against particle diameter in Figure 36. The biggest losses are for particles around 20 nm nominally 60 %. This copies the size distribution in Figure 33. For particles around 50-100 nm the values vary from 10 % losses to 10 % gain. Larger particle losses are increasing till 200 nm, with losses just under 40 % and then decreasing to 20 %.

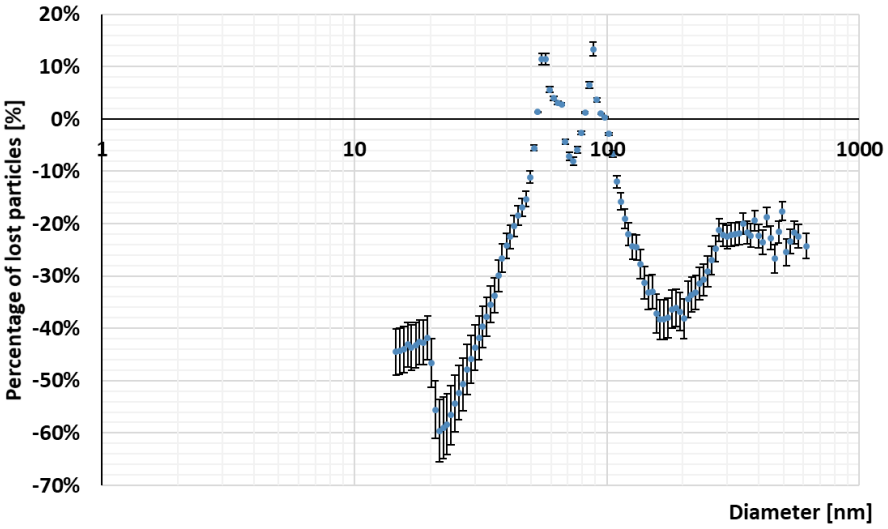

Figure 36: Dependency of iron particle losses on particle diameter

The comparison of the EEPS and the SMPS measurement can be seen in Figure 37. The biggest particle concentration is around 11 nm for the EEPS spectrum, while for the SMPS instrument it is around 22 nm.

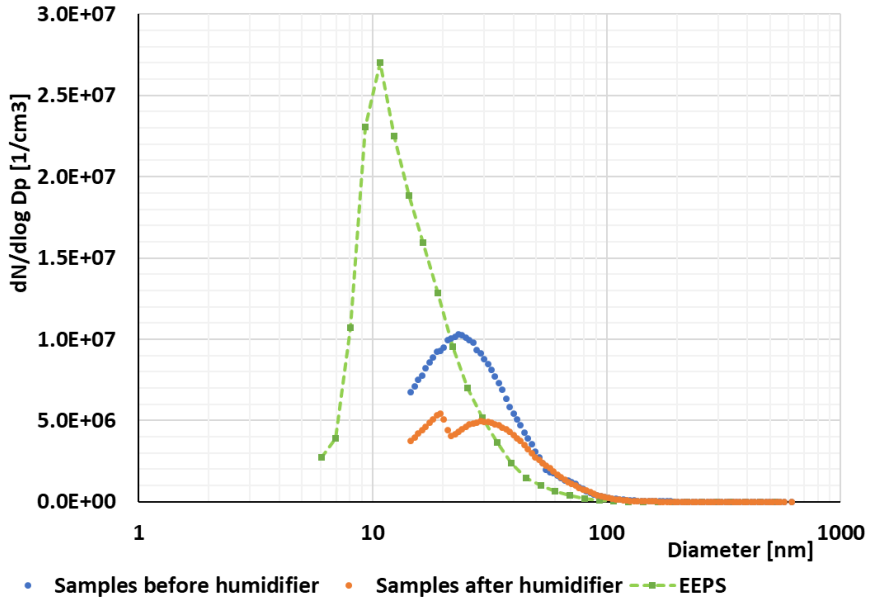

Figure 37: Comparison of mean particle size distribution of iron particles on the EEPS and on the SMPS. The EEPS was sampling from the PG outlet

To compare the size distribution from the EEPS and the SMPS from the same sampling after the PG, the EEPS spectrum was cut to range from 14.3 nm to 523 nm. This comparison is shown in Figure 38.

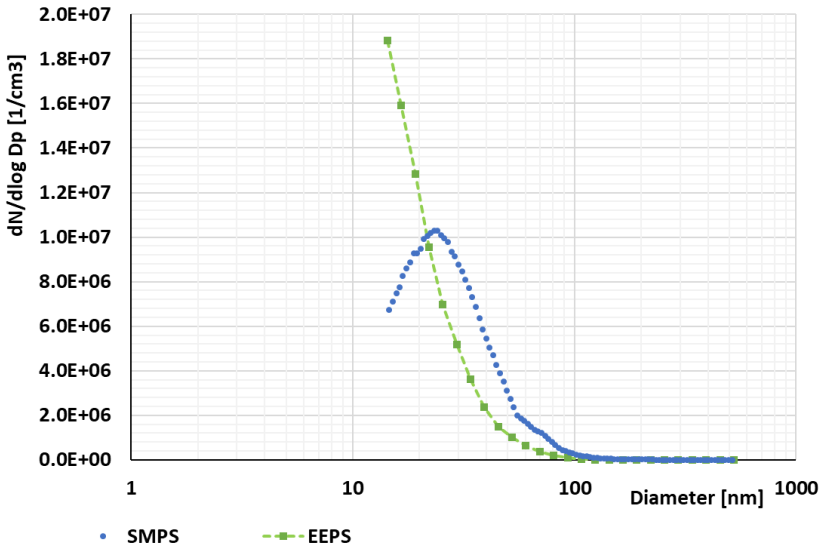

Figure 38: Comparison of size spectra from the EEPS and the SMPS on the same sampling spot

7.1.4. Carbon electrodes

In Figure 39, concentrations measured by the SMPS were plotted as a function of particle diameter. Two dashed lines represent missing parts of spectra. There are visible jumps around 25-30 nm and around 100 nm. These are caused by the CPC switching

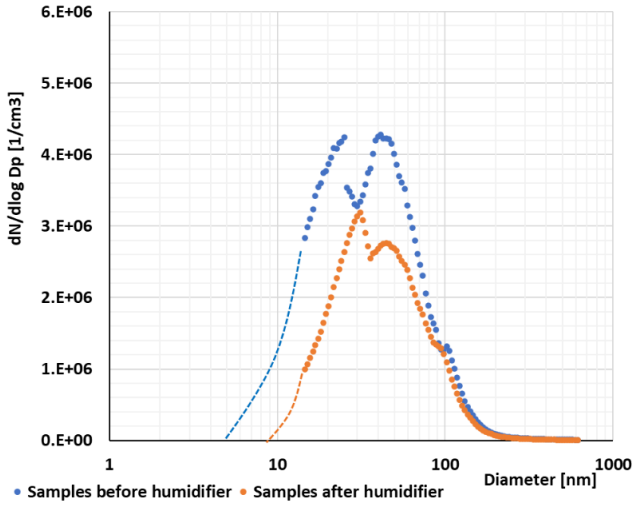

Figure 39: Mean particle size distribution of carbon particles before and after humidifier. The SMPS was sampling from the PG outlet for "Samples before humidifier", and from the humidifier outlet for "Samples after humidifier"

between different measuring modes. These curves were smoothed out by multiplying the concentrations in photometric measuring mode (between 25-90 nm) by an empirical calibration factor 1.5. After that plot in Figure 40 was obtained.

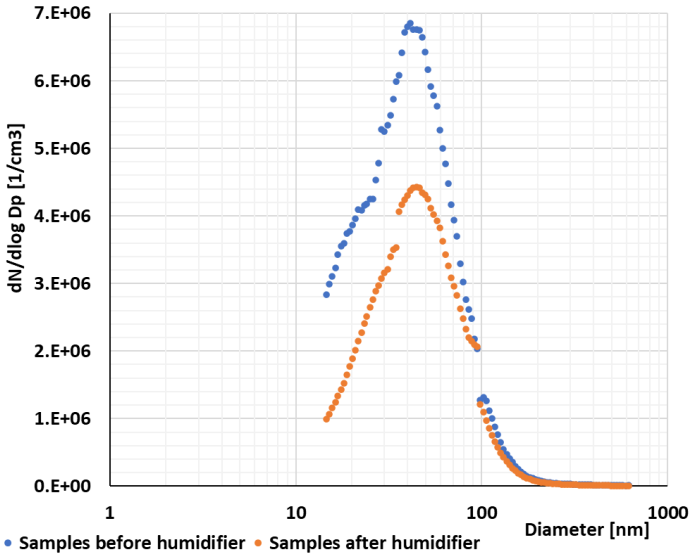

Figure 40: Concentrations of carbon particles measured by the SMPS multiplied by empirical calibration factor

Carbon electrodes produced particles with geometrical mean value of diameter 38.107±1.793 nm. After the humidifier the particle size was 41.150±1.768 nm. Particles were 7.99 % bigger after the membrane humidifier.

	Samples before the humidifier	Samples after the humidifier	Difference [%]
Geo. Mean [nm]	38.107	41.150	7.99
Geo. Std. Dev. [nm]	1.793	1.768	

Table 3: Geometrical mean value of carbon particle diameter. Geometric standard deviations represent variance among approximately 4 hours of testing.

Concentrations on the humidifier outlet (obtained from SMPS samples) were 31.93 %, 30.18 %, 21.65 %, 24.43 %, 19.51 %, 30.94 %, 37.02 %, 34.14 % and 27.41 % (28.58±5.81 %) lower than on the PG outlet. The mean total concentration measured by the EEPS was determined as 5,25±1,2 million #/cc.

The dependency of losses on particle diameter is shown in Figure 41. The biggest losses are for the smallest particles. Nominally 15 nm and 60 % of losses. With increasing diameter, the losses are decreasing till 30 nm. For particles around 40 nm the losses are around 40 %. For larger particles the losses are fluctuating around 20-30 %.

The comparison of full spectrum of the EEPS can be seen in Figure 42. The right side of the spectrum is almost identical for the EEPS and the samples before humidifier

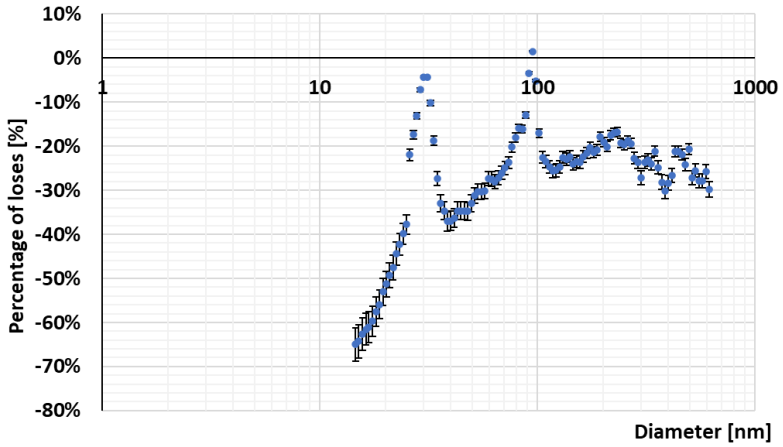

Figure 41: Dependency of iron particle losses on particle diameter

from the SMPS. The peak concentration from the EEPS is 1.5 times bigger than for the SMPS. The peak is also moved slightly to the smaller diameters around 22 nm. SMPS curves have their peaks around 35-40 nm.

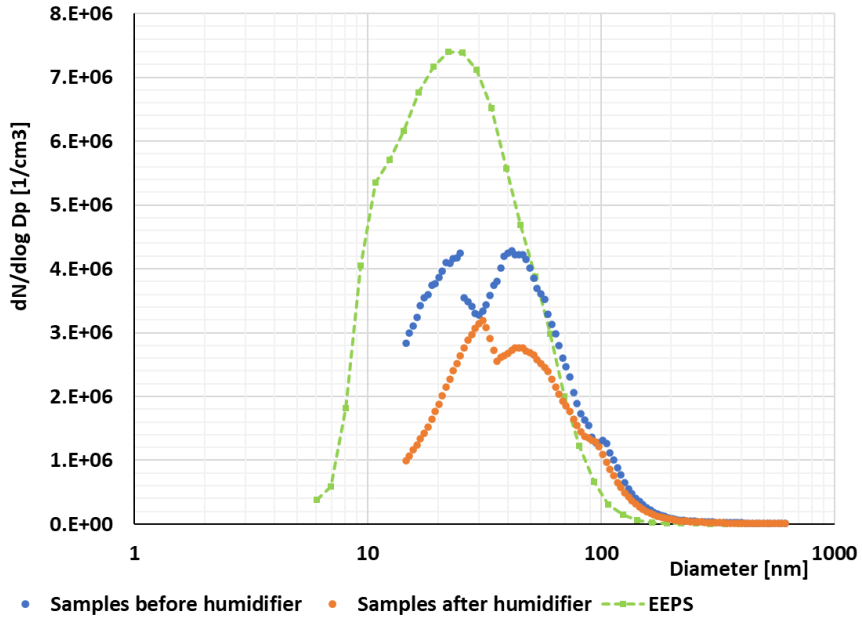

Figure 42: Comparison of mean particle size distributions of carbon particles on the EEPS and on the SMPS. The EEPS was sampling from the PG outlet

Comparison of the same size spectra is shown in Figure 43. By multiplying the concentration from the SMPS measured during the CPC photometric mode, a plot in Figure 44 was obtained. In Figure 44 can be seen that the peak of concentration from the EEPS and from the SMPS only by 0.5E+06 #/cc.

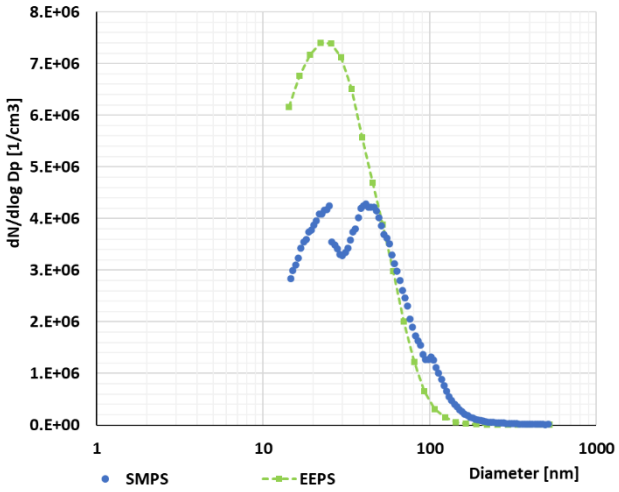

Figure 43: Comparison of spectra from the EEPS and the SMPS on the same sampling spot

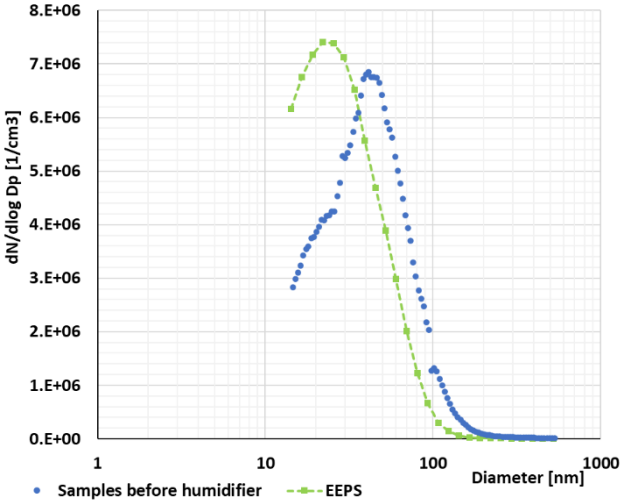

Figure 44: Comparison of the same size spectrum from the EEPS and the corrected SMPS spectrum

7.1.5. Comparing Au, Cu, Fe, and C

Mean particle size distribution of all elements (Au, Cu, Fe, C) before and after the humidifier can be seen in Figure 45. Size distribution of gold particles is the only one that does not have the peak visible. Because of that the difference between the curves before

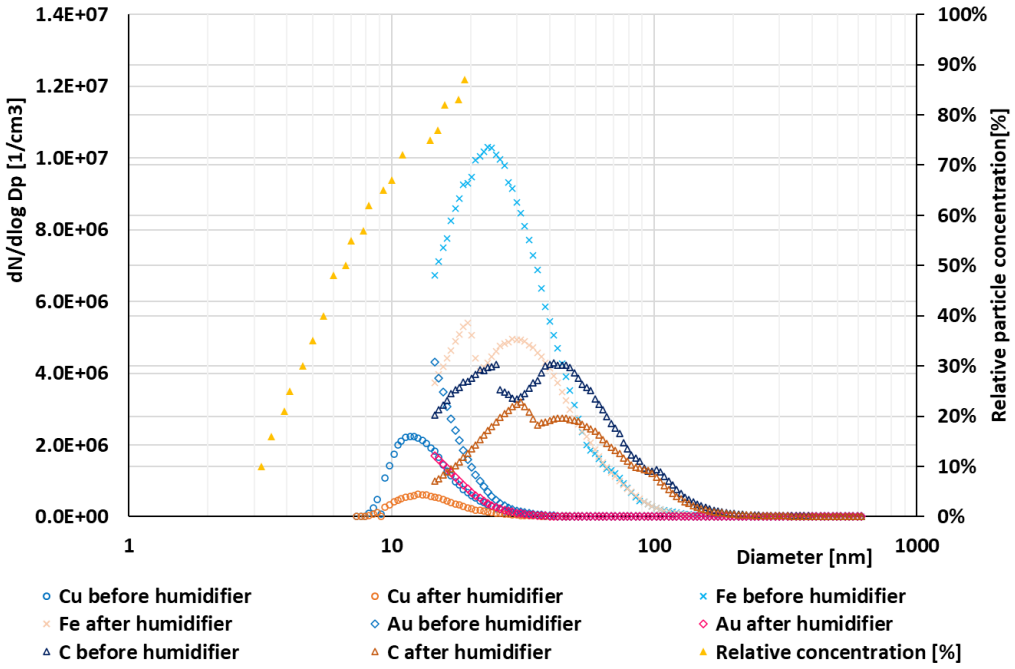

Figure 45: Mean particle size distributions from the SMPS. Concentrations of copper were multiplied by the relative concentration curve [38]. The samples before humidifier were collected from the PG outlet, samples after humidifier were collected from the humidifier outlet

and after humidifier for gold particles is not as significant as it is for iron for example. Concentration of copper were multiplied by curve “Relative particle concentration”.

The highest concentrations were measured for iron particles; the peak concentration was around 10^7 #/cc. The largest particles were measured for carbon electrodes.

The trend for gold and copper is that for particles larger than 30 nm concentrations are very low compared to the smaller particles. For iron and carbon, the particles reach up to 100 nm before the concentrations start to appear like a zero in the plot.

Losses for all materials are plotted in Figure 46. Some similarities can be seen. For all materials the losses are decreasing with increasing diameter till around 30-40 nm. Gold and copper particle losses became unstable for particle larger than 100 nm.

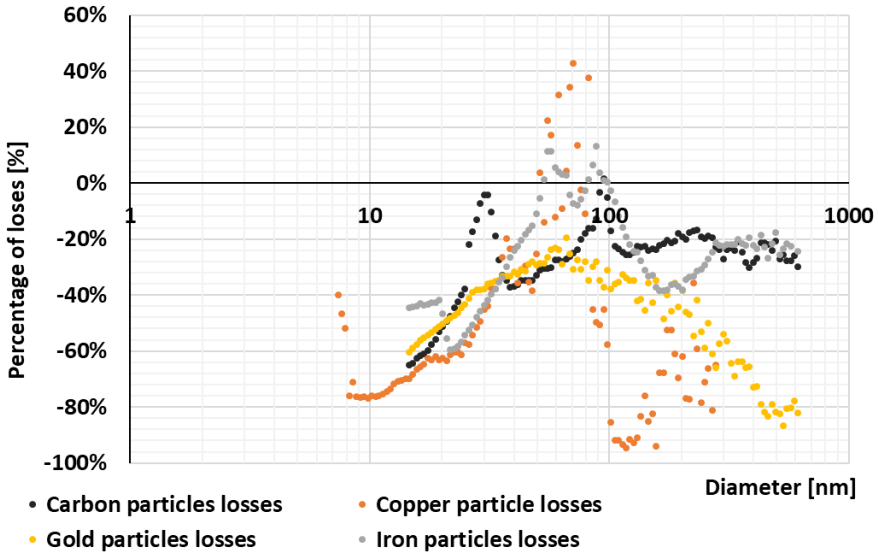

Figure 46: Losses of particles in percentages for all materials determined from total concentration on the SMPS

7.2. Losses in the RDD

The resulting file from the EEPS consisted of concentrations in each size channel during time of the measurement. The EEPS scans every second. The RDD was used in 7 cycles and 7 cycles were chosen from measurements without the RDD for comparison. Values were averaged through whole cycle and then compared with other cycles. Two of the 7 cycles were cold start and 5 of them were hot start.

Plot for measurement with the RDD is in Figure 47. The first peak is high concentration of primarily particles, the second one is made of agglomerates. For particles bigger than 100 nm the concentration is decreasing. For particles larger than 200 nm the concentrations are in units of particles per cc.

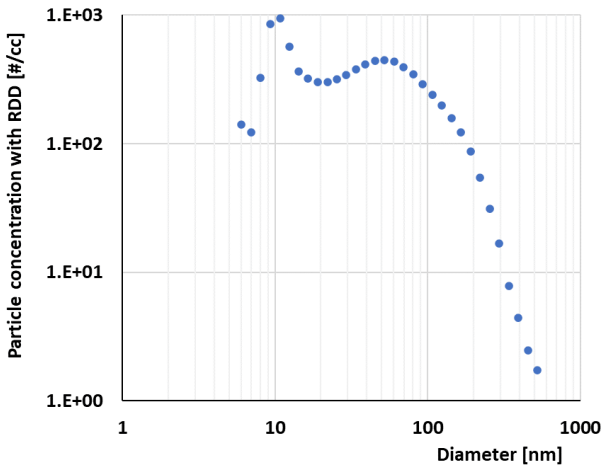

Figure 47: Mean particle size distribution for measurement with the RDD

For measurement without the RDD, the plot is in Figure 48. The primarily particles are around the same size, 10 nm, but the agglomerate peak can be seen in larger diameters around 350 nm.

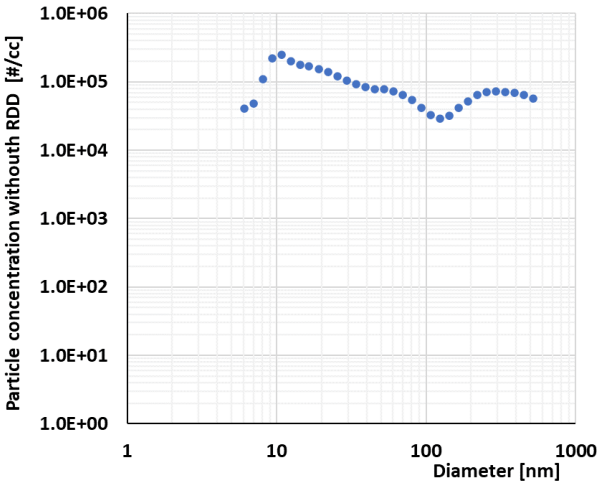

Figure 48: Mean particle size distribution for measurement without the RDD

The total concentration was obtained from the provided values from the EEPS. Those values were averaged through the whole cycle and then compared to the values from cycle with same type of start (cold-cold or hot-hot). Concentrations with the RDD (the EEPS was sampling on the outlet of the RDD) were 44.15 %, 51.79 %, 60.50 %, 37.52 %, 60.12 %, 61.64 % and 57.76 % (53.35±9.34 %) lower than when measuring without the RDD (the EEPS sampling on the outlet of the dilution tunnel).

Dependency of particle losses on particle diameter can be seen in Figure 49. The highest losses are for largest particles with diameter greater than 100 nm. The losses in

this area are more than 98 %. For particles with diameters from 80-100 nm the losses are in positive values up to 20 %. For particles with highest concentration, diameter around 10-15 nm, the losses were at 70 %.

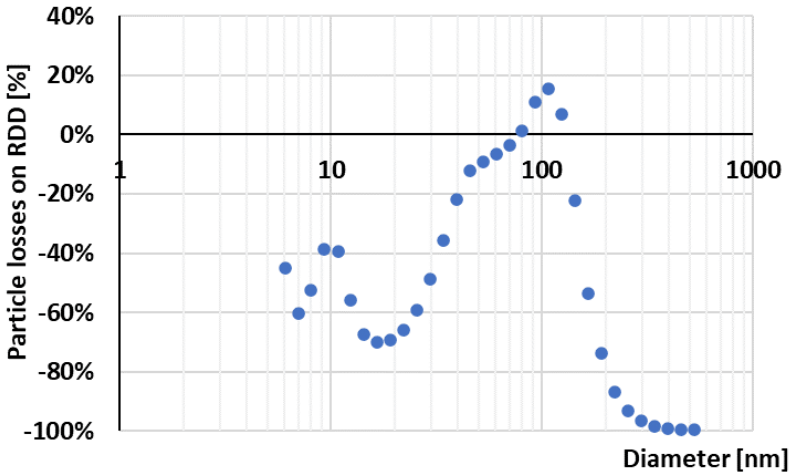

Figure 49: Particle losses as a function of particle diameter

8. Portable toxicological incubator

The toxicological incubator of smaller dimensions can be seen in Figure 50. This incubator has the capacity for four exposure chambers (See Figure 20).

Figure 50: Portable toxicological incubator; [author: Tereza Červená]

The amount of CO_2 needed to ensure 5 % on the cell cultures can be calculated. A flow of 0,2 lpm goes through the exposure chamber, therefore 0,01 lpm of CO_2 is needed for 1 exposure chamber. For four rounds of 240 minutes long exposure with four exposure chambers are therefore needed 38.4 liters of gaseous CO_2. The density of a gas phase of

CO_2 is 1.977 kg/m^3 [17] which means, that 76.31 grams are needed to complete the experiments.

A small high-pressure cylinder for food processing industry will be used for easy manipulation. A high-pressure cylinder with 500 grams of CO_2 can be seen in Figure 51. This cylinder is equipped with a valve with a W21,8x1/14" screw thread. The dimensions of this cylinder are 520x60 mm (length x diameter). [42]

Figure 51: High-pressure cylinder for 500 g of CO_2 [42]

A silicon tube with an outer diameter 6 mm and an inner diameter 4 mm will be used to connect the pressure regulator on the cylinder to the inlet of the incubator. The regulator allows a simple connection for the silicon tube (see Figure 52). For connection with sample flow, a "Y" plastic connector will be used.

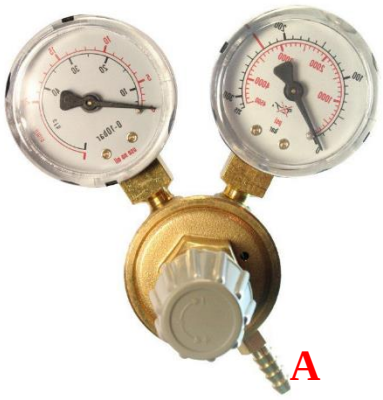

Figure 52: The CO_2 pressure regulator; (A) connection of the silicon tube [47]

Another silicon tube 4/6 mm will be used for connection between the "Y" connector and the heat exchanger inlet. As a heat changer an aluminum tube – EN 573-3 AW 6060 T6, 6x1 mm will be used. The maximum length that will fit in the incubator is 30 cm. Two heat exchangers are needed, one for the sample and one for reference.

Humidifiers used in both experiments are positioned on laboratory stands approximately 30 cm tall. This is not a setup that could be used in the portable incubator because of its size and possible instability during driving tests. Water reservoirs are larger than needed for 240 minutes experiments across four days. Relative humidity ϕ can be calculated as follows

$$\phi = \frac{m}{M} \tag{5}$$

where m is the density of water vapor at relative humidity and M is the density of water vapor in fully saturated air at a given temperature. M at 37 °C can be found in thermodynamic tables as 43,92 g/m^3 [43]. After substitution for ϕ=90 %, it is possible to get that m=39.53 g/m^3 of water vapor.

Th flow through both humidifiers is 1.1 lpm (four exposure chambers, 0.2 lpm each, plus 0.3 lpm for sampling), for the whole experiment 1.056 m^3 of air at 90 % relative humidity will be needed, therefore around 41.74 g of water is needed in total. Water reservoirs should have a volume of 25 milliliters each.

To achieve the necessary limit of humidity the reservoir needs to be always installed on top of the humidifier. Since the amount of space in the portable incubator is limited, the water reservoir needs to be 5 centimeters tall at maximum. Cylindrical shaped reservoirs with diameter 2.5-3 cm and 5 cm tall will be used.

Humidifiers will be placed in clamps with rubber lining. Inner diameter can be adjusted by 2 screws from 40 to 45 mm. This clamp is equipped with head with M8 screw thread. ISO 4017 M8-40 mm full thread bolt will be used to hold the clam in place. The bolt will go through aluminum "T" profile - EN 573-3 AW 6060 T66, 100x60x5 mm and will be secured with ISO 4032 M8 nut and ISO 7089 M8 plain washer. Both humidifiers will be installed on one "T" profile. Two plain holes with diameter 8.2 mm need to be drilled to the "T" profile. Their placement is demonstrated in Figure 53.

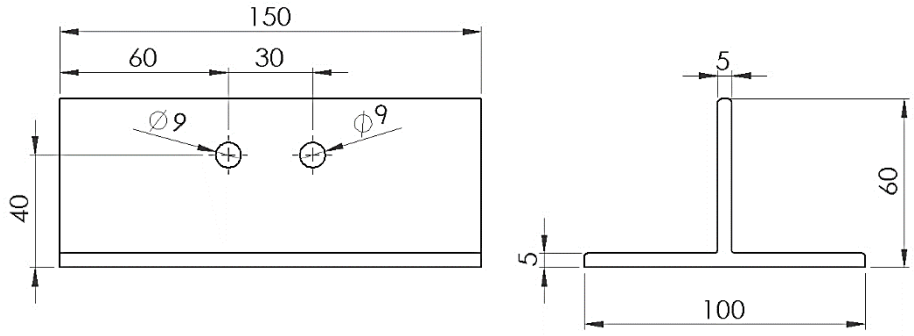

Figure 53: "T" profile with holes for placement of 2 bolts

All necessary parts, needed to assembly the portable toxicological incubator, including the providers are listed in Table 4.

Name	**Dimensions**	**Provider**	**Catalog n.**	**Quantity**
CO_2 cylinder	500 g	**Sifos-obchod**; available at: www.sifos-obchod.cz	TL00500	1
CO_2 regulator	W21/8”	**Ivital**; available at: www.rostlinna-akvaria.cz/eshop/	504	1
Silicon tube	4/6 mm	**Gumex**; available at: www.gumex.cz	00017044	3 meters
“Y” connector	6 mm	**Tafimex**; available at: www.tafimex.cz	30306	1
Aluminum tube	6x1x300 mm	**Ehlinik.cz**; available at: www.ehlinik.cz	194001808	2
Clamp	40-45 mm, M8	**Dek**; available at: www.dek.cz	298K6	2
ISO 4017 full thread bolt	M8-40 mm	**Obchodprodilnu.cz**; available at: www.obchodprodilnu.cz	0505106	2
ISO 4032 nut	M8	**Obchodprodilnu.cz**; available at: www.obchodprodilnu.cz	0542010	2

ISO 7089 plain washer	M8	**Obchodprodilnu.cz**; available at: www.obchodprodilnu.cz	0551010	2
Aluminum "T" profile	100x60x5 length 150 mm	**Ehlinik.cz**; available at: www.ehlinik.cz	06-0014	1

Table 4: List of parts that are needed to assembly the prototype of the potable toxicological incubator

9. Discussion

Losses in an exposure chamber sampling train were determined in two experiments setups. Losses in the membrane humidifier were examined with the PG and losses in the RDD were determined with a diesel engine. Losses in the membrane humidifier were also determined in study [2].

A gasoline engine (Škoda Auto 1.4 TSI, EA211 CHP) was used as a producer of particles in study [2]. This study determined particle losses on the membrane humidifier PermaPure model no. FC125-240-5MR with the CPC sampling on the exposure chamber inlet and the EEPS sampling on the RDD outlet. Particle losses were determined as a difference between the concentration on the EEPS and the CPC. The EEPS concentration was corrected to the CPC concentration. The average CPC concentration was 40.3±2.1 % lower than the EEPS concentration. Losses were also obtained by comparing the CPC measured concentrations on the exposure chamber inlet vs. concentrations on the proportional diluter outlet. Mean particle concentration losses determined by this way were 36.9±3.8 %.

The losses for carbon particles, when the PG was used, were 28.58±5.81 %. The result is similar to the one presented in study [2]. Bigger losses in study [2] might be caused by a longer sampling train, particles might get caught on the walls. Another reason might be, that the PG generates pure particles with a surface free of any organic materials, and therefore particles can behave differently, can react differently than the ones from the ICE. Another reason for the values to vary is that even though that carbon particles are particles with the highest concentration in the engine exhaust, other particles can also be present, such as particles from corrosion, or there could be some contamination in the proportional diluter. After comparing these results, it can be generally stated, that around 1/3 of carbon-based particles are lost in the membrane humidifier PermaPure model no.

FC125-240-5MR. Particle losses for gold (44.51±7.89 %) and iron (36.69±9.96 %) were also quite similar to the ones in study [2]. Losses for gold particles were evaluated from the smallest spectrum. If the whole spectrum was covered, it is possible than the losses would be different. Since the biggest lost in particle concentration is for the mean value of diameter, it could be assumed that losses for gold particles would be similar to copper particles losses. Losses for copper particles were the biggest (68.05±1.42 %), this might be caused by small particle size (mean value around 10-12 nm).

Iron and copper are stated as one of the components of braking pads in study [32] and review paper [44]. The iron and copper fibers represent one of the main friction materials of semi metallic braking pads [44]. Therefore, their inclusion in this master's study makes sense because these can have a potentially dangerous effect on human health. The author is not aware of a way how a vehicle could produce gold particles, but since gold is very chemically stable element, it can be used as a reference.

In study [2], the mean particle size distribution was measured (Figure 54). A strong peak at 10 nm can be seen when the EEPS was sampling from the gravimetric sampling system. The study supposes that a nucleation takes place because the low dilution ratio causes the strong peak. The second peak for agglomerate particles is not as strong as the first one. This corresponds to the peak in size distribution measured for carbon particles in Figure 40.

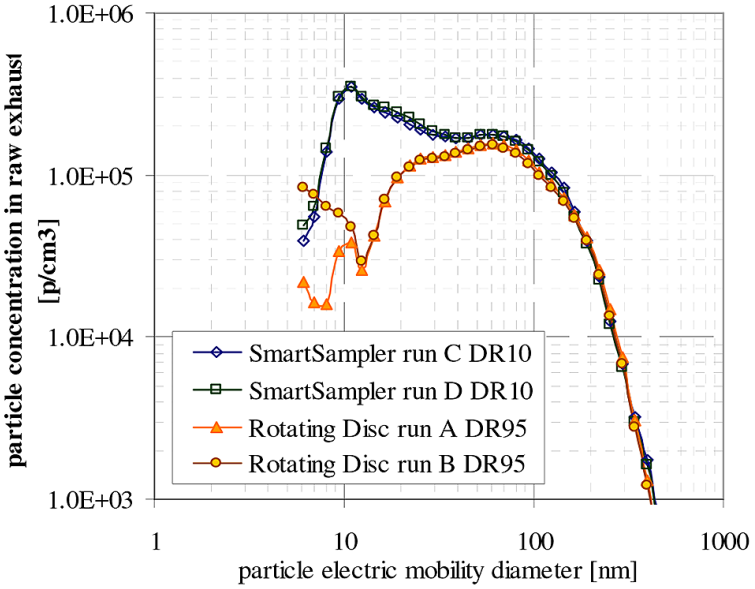

Figure 54: Mean particle size distribution over WLTC as measured by the EEPS sampling from the RDD and from proportional gravimetric sampling system [2]

The peak in Figure 40 is at around 35-45 nm. This difference is probably caused by a production of cleaner particles in the PG. Another reason might be that the sampling train for the experiment with the PG was shorter. In study [2] the sample needed to pass through multiple rooms with tens of meters of sampling train. With the PG, the sample only went through a sampling train around units of meters or tens of centimeters long and therefore did not have enough time to fully agglomerate.

The effect of the engine exhaust was also examined in study [3]. Standard direct injection gasoline engine, used in Škoda Octavia (Škoda Auto 1.4 TSI, EA211 CHP), fueled with standard gasoline (BA-95N, Čepro, 4.9% ethanol, 0.3% ETBE, referred to as E5), was used for producing sample flow. The engine was driven on engine dynamometer. The sampling ran during the WLTC test. The engine exhaust was examined during cold and warm start. Engine exhaust was diluted with fresh air with ratio 10:1.

The mean particle concentration was determined from the electrical mobility of particles (the EEPS, TSI, in diluted exhaust and corrected to DR) and from the aerodynamic diameter (electrostatic Low-pressure Impactor, Dekati, high-temperature version running at 160 C, in undiluted exhaust). The mean particle concentration was determined as 5-8 million of #/cc for the cold start and around 2 million #/cc for the hot start.

In this thesis, the mean particle concentration of carbon particles determined from total concentration on the EEPS was 5,25±1,2 million #/cc. The values are more similar to the cold start test. If the PG must simulate the warm start, some form of dilution would be necessary to reach smaller concentrations. Only carbon particles are considered for comparing with real engine exhaust because those represent the major part emitted from the engine.

The possibility of using the RDD (type MD-19, Matter Engineering, n. 101496, number of disc: 69090/12/01/36, date 17.9.2013) with the PG was also examined. A problem with the RDD occurred during the experiment. A layer of particles was found after disassembling the RDD (See Figure 55 before cleaning and Figure 56 after). The RDD disc might be damaged because of that. Due to this fact, the question if RDD can be used in this setup arises. It is not clear if the particles accumulated during the experiment with the PG or during the previous experiment with the engine.

Figure 55: Clogged and possibly damaged parts of the RDD

Figure 56: Parts of the RDD after cleaning

Concentrations with the RDD measured by the EEPS in chapter 7.2 are averaged over the whole cycle WHTC. For the EEPS, the detectable limit is around 10^3 (#/cc) for a particle size 7 nm (see Figure 57). Average concentrations in Figure 47 are very low (peak is around 1000 #/cc) when compared to the detectable limit. It is safe to assume that a lot of values were below the detectable limit. Losses calculated from these values

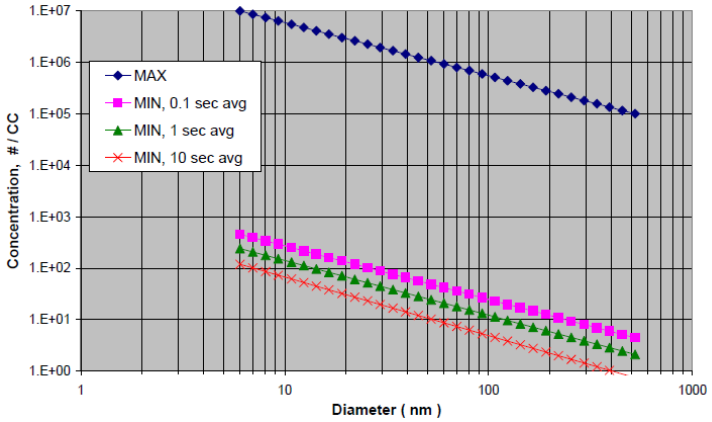

Figure 57:Minimum and maximum detectable concentration for the EEPS [34]

were around 50%. The final losses are 5 times bigger than in study [45] or user manual [40].

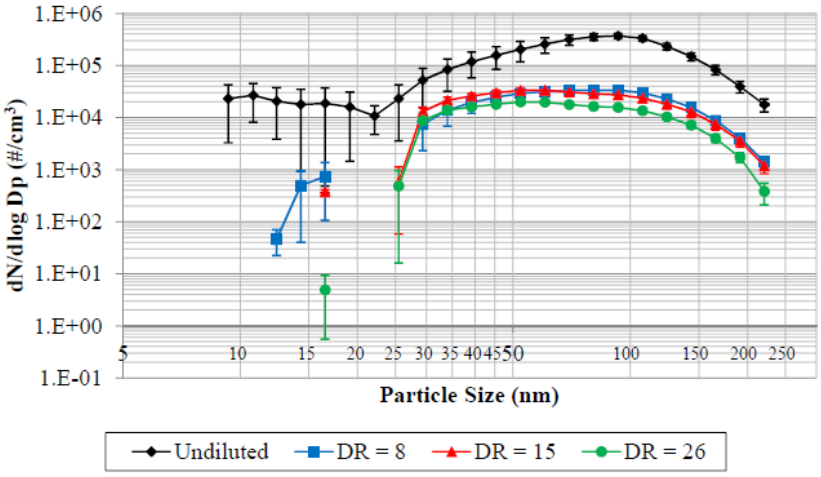

Figure 58: Engine exhaust particle distribution at various dilution ratio for the Single-Stage TSI diluter [45]

Particle losses in multiple aerosol diluters were estimated in study [45]. The single-stage and the two-stage TSI 379020A rotary disk thermo/diluters and Dekati FPS-4000 ejector were used. Particles were generated from a Tier 1 direct injection, turbocharged, water-cooled Cummis CI engine. The engine was operating in stabilized condition at mode 9 of the ISO 8178 test (1400 rpm, 25 % load). The EEPS and FMPS (Fast mobility particle sizer) were used for analysis of particle concentration upstream and downstream of the diluters. Results for single-stage TSI diluter can be seen in Figure 58. Particles smaller than 30 nm were lost during the dilution process. Concentrations of particles larger than 30 nm were stable with 99.7 % confidence. From the difference between the black (undiluted) curve and the diluted curves, it can be said that undiluted concentrations were about 10 % higher than undiluted concentrations.

Study [45] determined particle concentrations in undiluted exhaust. Concentrations for particle size around 100 nm were around 120 000 #/cc. Values for particles smaller than 30 nm were determined with higher deviation with mean values around 11 000 #/cc. In this thesis (Figure 48), particle concentrations for particles larger than 100 nm were determined as 90 000 #/cc, for particles around 10 nm it was 110 000 #/cc. While the difference in larger particles is not as big (30 000 #/cc), for smaller particles it is quite significant – one order higher. This difference is caused by a particle agglomeration of small particles.

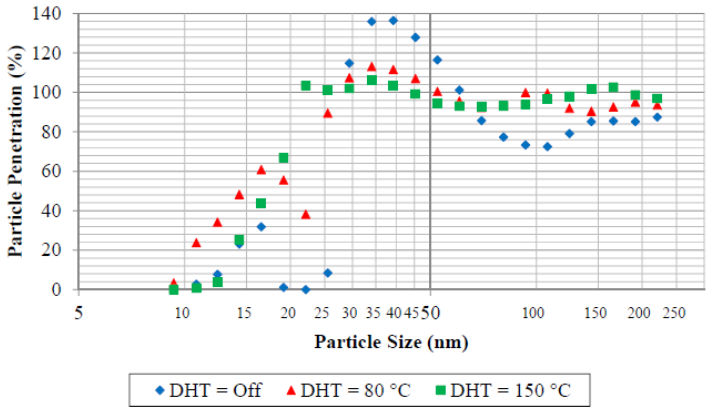

Figure 59: Engine exhaust particle penetration corresponding to the primary dilution air temperature for the single-stage TSI diluter [45]

Experiments with a rotation disc thermodiluter were also carried out in study [45]. Particle penetration can be seen in Figure 59. A gain in particle concentrations can be observed in area around 30-70 nm when the heating was turned off. But even with heating turned on there can be found values above a 100 %. The increase in particle concentration can be seen in Figure 46 and Figure 49 in this thesis. Only copper and iron particles show this phenomenon in Figure 46, in area with diameters around 50-100 nm. In Figure 49 the increase for engine exhaust particles is from 80 to 150 nm.

For particles larger than 50 nm, the particle penetration was determined around 80-98 % [45]. In this thesis particle losses in the RDD were determined as 53.35±9.34 %. The reason for this is that concentrations downstream of the RDD were below the EEPS detectable limit. The EEPS evaluated these concentrations as 0 and the average concentration was reduced.

Mean atmospheric particle concentrations in traffic impacted area were determined in study [46]. Mean particle number concentrations close to the traffic intersection and on the sideroad were 48 to 180 thousand #/cc depending on the weather. Mean concentrations in the park with no vehicular influence were determined as 8 750 #/cc on cold days and around 30 000 #/cc on hot days. Those values are several orders higher than values measured with the RDD in the chapter 7.2.

New setup for the membrane humidifier is described in chapter 8. In this setup two membrane humidifiers are installed on one aluminum “T” profile. This will ensure stability. The humidifier is necessary to obtain sufficient humidity to simulate the environment in human lungs.

10. Conclusion

Due to the increasing air pollution, knowing its effects on human body is key to understand how to protect and how and why to reduce emission production. The portable toxicological incubator is needed to examine effect of engine exhaust in real time and real-life situations to cells. The air-liquid interface is now commonly used method to examine effect of aerosol samples on cellular cultures. This thesis reviews composition of the vehicular exhaust as well as mechanism of formation of exhaust gases and particles, losses in the exposure chamber sampling train, and design of the portable toxicological incubator.

Experiments to determine losses in the membrane humidifier PermaPure model no. FC125-240-5MR were done with the particle generator VSP-G1. The membrane humidifier is needed to maintain 80-95 % relative humidity. Concentrations were measured by the scanning mobility particle sizer with condensation particle counter. Size distribution and particle concentration were obtained from these instruments. Losses were determined as a difference between total particle concentrations upstream and downstream from the humidifier. Those losses were determined as 44.51±7.89 % for gold, 68.05±1.42 % for copper, 36.69±9.96 % for iron and 28.58±5.81 % for carbon. Concentrations upstream of the humidifier were compared to concentrations measured by the engine exhaust particle sizer sampling from the same spot. Biggest particles were measured for carbon with geometric mean value of diameter 38.1±1.8 nm upstream of the humidifier and 41.2±1.8 nm downstream of the humidifier. Smallest particles were generated for gold with mean value of diameter around 10 nm which was obtained by the EEPS, because the SMPS was set up to measure particles above 14 nm.

Losses in the rotation disc diluter type MD-19, Matter Engineering, n. 101496, number of disc: 69090/12/01/36 could not be sufficiently determined. The diluter was connected to a dilution tunnel, which was maintaining constant volume sample from diesel engine Iveco Tector. Particle concentrations measured from the diluter outlet were lower than atmospheric concentration. Determined losses were around 50 %, which is about five time more than assumption.

It was shown that particle losses depend on a particle size. The biggest losses are for particles smaller than 30 nm. Concentrations downstream of the humidifier for particle sizes 80-100 nm are higher than concentrations upstream. This can be caused by

condensation or agglomeration. For particles bigger than 100-200 nm concentrations are unstable and not reliable.

To ensure a constant volume sample the exhaust needs to be diluted. Traditional diluters (such as dilution tunnel) are big and are not suitable for on-board measuring. The rotating disc diluter could be theoretically sufficient but other tests are needed to ensure that the RDD will not be clogged.

A small CO_2 cylinder will be part of the portable toxicological incubator. It was calculated that 500 g of CO_2 will be sufficient to complete experiments. Small size and low weight allow easy manipulation. As stated above humidifier is crucial to maintain humidity in the exposure chamber. Two membrane humidifiers will be mounted to the aluminum “T” profile to ensure their stability during driving tests. Water reservoirs will be replaced with smaller ones with 25 milliliters volume.

References

[1] Health Effect Institute, "State of Global Air," 2018. [Online]. Available: https://www.stateofglobalair.org/sites/default/files/soga-2018-report.pdf. [Accessed October 2021].

[2] Vojtisek-Lom, M., Pechout, M., Macoun, D., Rameswaran, R. et al., "Assessing Exhaust Toxicity with Biological Detector:Configuration of Portable Air-Liquid Interface Human Lung Cell Model Exposure System, Sampling Train and Test Conditions," *SAE Technical Paper*, Vols. 2019-24-0050, 2019; https://doi.org/10.4271/2019-24-0050.

[3] T. Cervena, M. Vojtisek-Lom and e. al., "Ordinary Gasoline Emissions Induce a Toxic Response in Bronchial Cells Grown at Air-Liquid Interface," *International Journal of Molecular Sciences*, vol. 22 (1), p. 79, 2021; https://doi.org/10.3390/ijms22010079.

[4] Pavel Rossner Jr., Tereza Cervena, Michal Vojtisek-Lom, "In vitro exposure to complete engine emissions – a mini-review," *Toxicology*, vol. 462, no. 152953, 2021; https://doi.org/10.1016/j.tox.2021.152953.

[5] University of Washington Institute for Health Metrics and Evaluation, Weltbank, *The Cost of Air Pollution Strengthening the Economic Case for Action*, 2016.

[6] International Agency for Research on Cancer and World Health Organization, *IARC Monographs on the Evaluation of Carcinogenic Rosk to humans Diesel and Gasoline Engine Exhaust and Some Nitroarenes*, 2013.

[7] Cao, X., Coyle, J.P., Xiong, R., Wang, Y., Heflich, R.H., Ren, B., Gwinn, W.M., Hayden, P.,, "Invited review: human air-liquid-interface organotypic," *In Vitro Cell.Dev.Biol.-Animal*, vol. 57, pp. 104-132, 2021; https://doi.org/10.1007/s11626-020-00517-7.

[8] Loretta Müller, Pierre Comte, Jan Czerwinski, Markus Kasper, Andreas C. R. Mayer, Peter Gehr, Heinz Burtscher, Jean-Paul Morin, Athanasios Konstandopoulos, and Barbara Rothen-Rutishauser, 2010, "New Exposure System To Evaluate the Toxicity of (Scooter) Exhaust Emissions in Lung Cells in Vitro," *Environmental Science & Technology*, vol. 44 (7), pp. 2638-2638, 2010; https://doi.org/10.1021/es903146g.

[9] J. Macek, Spalovací motory I, Praha: Nakladatelství ČVUT, 2007.

[10] J. Heywood, Internal Combustion Engine Fundamentals, McGraw-Hill, 1988.

[11] Kamil, Mohammed & Ramadan, Khalid & Ghenai, Chaouki & Olabi, Abdul & Nazzal, Ibrahim, "Emissions from Combustion of Second-Generation Biodiesel Produced from Seeds of Date Palm Fruit (Phoenix dactylifera L.)," *Applied Sciences*, Vols. 9, 18:3720, 2019; https://doi.org/10.3390/app9183720.

[12] M. Takáts, *Měření emisí spalovacích motorů,* 1997, ISBN 80-01-01632-3.

[13] Wikipedia, "Carbon monoxide," 2021. [Online]. Available: https://en.wikipedia.org/wiki/Carbon_monoxide. [Accessed November 2021].

[14] The NHS website - NHS, "Carbon monoxide poisoning," Crown copyright, [Online]. Available: https://www.nhs.uk/conditions/carbon-monoxide-poisoning/. [Accessed December 2021].

[15] WikiSkripta, "Karbonylhemoglobin," 2018. [Online]. Available: https://www.wikiskripta.eu/w/Karbonylhemoglobin. [Accessed November 2021].

[16] MayoClinic, "Carbon monoxide poisoning," 1998. [Online]. Available: https://www.mayoclinic.org/diseases-conditions/carbon-monoxide/symptoms-causes/syc-20370642. [Accessed November 2021].

[17] Wikipedia, "Carbon dioxide," 2021. [Online]. Available: https://en.wikipedia.org/wiki/Carbon_dioxide. [Accessed November 2021].

[18] Britannica, "Carbon dioxide," Encyclopedia Britannica, 2020. [Online]. Available: https://www.britannica.com/science/carbon-dioxide. [Accessed November 2021].

[19] N. Climate.gov, "Climate Change: Atmospheric Carbon Dioxide," 2020. [Online]. Available: https://www.climate.gov/news-features/understanding-climate/climate-change-atmospheric-carbon-dioxide. [Accessed November 2021].

[20] F. A. Carey, "Hydrocarbon," Encyclopedia Britannica, 2020. [Online]. Available: https://www.britannica.com/science/hydrocarbon. [Accessed December 2021].

[21] Mao-wen Weng, Hyun-Wook Lee, Sung-Hyun Park, Yu Hu, Hsing-Tsui Wang, Lung-Chi Chen, William N. Rom, William C. Huang, Herbert Lepor, Xue-Ru Wu, Chung S. Yang, Moon-shong Tang, "Aldehydes are the predominant forces inducing DNA damage and inhibiting DNA repair in tobacco smoke carcinogenesis," *Proceedings of the National Academy of Sciences,* vol. 115, 2018; https://doi.org/10.1073/pnas.1804869115.

[22] Amaj Ahmed Laskar & Hina Younus, "Aldehyde toxicity and metabolism: the role of aldehyde dehydrogenases in detoxification, drug resistance and carcinogenesis," *Drug Metabolism Reviews,* vol. 51:1, pp. 42-64, 2019: https://doi.org/10.1080/03602532.2018.1555587.

[23] Agency for toxic substances and disease registry, "Medical Management Guidelines for Nitrogen Oxides," [Online]. Available: https://wwwn.cdc.gov/TSP/MMG/MMGDetails.aspx?mmgid=394&toxid=69. [Accessed December 2021].

[24] S. Mohankumar, P. Senthilkumar, "Particulate matter formation and its control methodologies for diesel engine: A comprehensive review," *Renewable and Sustainable Energy Reviews,* vol. 80, pp. 1227-1238, 2017; https://doi.org/10.1016/j.rser.2017.05.133.

[25] Panu Karjalainen, Liisa Pirjola, Juha Heikkilä, Tero Lähde, Theodoros Tzamkiozis, Leonidas Ntziachristos, Jorma Keskinen, Topi Rönkkö, "Exhaust particles of modern gasoline vehicles: A laboratory and an on-road study," *Atmospheric Environment,* vol. 97, pp. 262-270, 2014; https://doi.org/10.1016/j.atmosenv.2014.08.025.

[26] A. Abdel-Rahman, "On the emission from internal combustion engines: A review," *International Journal of Energy Research,* vol. 22 (6), pp. 483-513, 1998; https://doi.org/10.1002/(SICI)1099-114X(199805)22:6<483::AID-ER377>3.0.CO;2-Z .

[27] Anetor, L., Odetunde, C. & Osakue, E.E., "Computational Analysis of the Extended Zeldovich Mechanism," *Arabian Journal for Science and Engineering,* vol. 39, pp. 8287-8305, 2014; https://doi.org/10.1007/s13369-014-1398-7.

[28] Michael Rößler, Amin Velji, Corina Janzer, Thomas Koch, and Matthias Olzmann, "Formation of Engine Internal NO2: Measures to Control the NO2/NOX Ratio for

Enhanced Exhaust After Treatment," *SAE International journal of engines,* vol. 10 (4), pp. 1880-1893, 2014; https://doi.org/10.4271/2017-01-1017.

[29] B. Chehroudi, Hydrocarbon Emission from Spark-Ignited Engines, 1997.

[30] E. &. P. V. Meloni, "Most Recent Advances in Diesel Engine Catalytic Soot Abatement: Structured Catalysts and Alternative Approaches," *Catalysts,* vol. 10, p. 745, 2020; https://doi.org/10.3390/catal10070745.

[31] X. Querol, A. Alastuey, M.M. Viana, et al., "Speciation and origin of PM10 and PM2.5 in Spain," *Journal of Aerosol Science,* vol. 35, pp. 1151-1172, 2004; https://doi.org/10.1016/j.jaerosci.2004.04.002.

[32] Piyush Chandra Verma, Mattia Alemani, Stefano Gialanella, Luca Lutterotti, Ulf Olofsson, Giovanni Straffelini, "Wear debris from brake system materials: A multi-analytical characterization approach," *Tribology International,* vol. 94, pp. 249-259, 2016; https://doi.org/10.1016/j.triboint.2015.08.011.

[33] Schwarze PE, Totlandsdal AI, Herseth JI, Holme JA,Låg M, Refsnes M, Øvrevik J, Sandberg WJ and Bølling AK, "Importance of sources and components of particulate air pollution for cardio-pulmonary inflammatory responses," in *Air Pollution*, Sciyo, 2010, pp. 47-62.

[34] TSI Incorporated, TSI 3090 EEPS™ Engine Exhaust Particle Sizer™ Spectrometer Manual, TSI Incorporated, 2015.

[35] TSI Incorporated, Updated Inversion Matrices for Engine Exhaust Particle Sizer (EEPS) Spectrometer Model 3090 Application Note EEPS-005, TSI corporated, 2015.

[36] TSI Incorporated, Particle instruments Aerosol Neutralizers, Series 3080 Electrostatic Classifiers, Operation and Service Manual, TSI Incorporated, 2009.

[37] TSI Incorporated, Model 3022A, Condensation Particle Counter, TSI Incorporated, 1999.

[38] Ankilov, A., Baklanov, A., Colhoun, M. et al.,, "Particle Size Dependent Response of Aerosol Counters," *Atmospheric Research,* Vols. 62(3-4), pp. 209-237, 2002; https://doi.org/10.1016/S0169-8095(02)00011-X.

[39] Bernemyr Hanna, "Volatility and number measurement of diesel engine exhaust particles.," KTH, School of Industrial Engineering and Management (ITM), Machine Design (Dept.), Machine Design (Div.)., 2007, ISBN 978-91-7178-753-8.

[40] Testo SE & Co. KGaA, "Testo MD19-3E user manual," Testo SE & Co. KGaA, 2016.

[41] A. Schmidt-Ott, "Building Blocks for Nanotechnology from Spark Ablation," 2021. [Online]. Available: https://vsparticle.com/fileadmin/user_upload/Building_Blocks_for_Nanotechnology_from_Spark_Ablation.pdf. [Accessed December 2021].

[42] SIFOS-obchod.cz, "Tlaková láhev CO2 0,5 kg (500 gramů) s ochranným košem W21,8x1/14," SIFOS-obchod.cz, 2022. [Online]. Available: https://www.sifos-obchod.cz/bombicky-co2-sifonove/tlakova-lahev-co2-0-5-kg-500-gramu-s-ochrannym-kosem-w21-8x1-14/. [Accessed January 2022].

[43] Doc. Ing. Bořivoj Ondra, CSc., Termomechanika a hydromechanika - Termodynamické tabulky, Vysoká škola zemědělská v Brně, 1991.

[44] J. Chandradass, M. Amutha Surabhi, P. Baskara Sethupathi, P. Jawahar, "Development of low cost brake pad material using asbestos free sugarcane bagasse ash hybrid composites," *Materials Today: Proceedings,* Vols. 45, part 7, pp. 7050-7057, 2021; https://doi.org/10.1016/j.matpr.2021.01.877..

[45] Terry Hoon Suk Jung , "Evaluation and Verification of Aerosol Diluters: Accuracy and Particle Loss," 2014.

[46] Ismael Luis Schneider, Elba Calesso Teixeira, Luis Felipe Silva Oliveira, Flavio Wiegand, "Atmospheric particle number concentration and size distribution in a traffic–impacted area," *Atmospheric Pollution Research,* vol. 6 (5), pp. 877-885, 2015; https://doi.org/10.5094/APR.2015.097.

[47] INVITAL Rostlinna-akvaria.cz, "CO2 redukční ventil se dvěma manometry," INVITAL Rostlinna-akvaria.cz, 2022. [Online]. Available: https://www.rostlinna-akvaria.cz/eshop/co2-do-akvaria/co2-redukcni-ventil-se-dvema-manometry. [Accessed January 2022].

List of figures

List of tables

Appendix

	Total particle concentration before humidifier	Total particle concentration after humidifier
	[#/cc]	[#/cc]
	593730	257208
	554006	254311
	506401	253492
	581674	257091
	528863	299732
	561085	269957
	475613	268499
	522370	278706
	542781	317849
	517068	292732
	438845	276360
	470604	310421
	505604	299228
	427718	294495
	476220	295853
Mean [#/cc]	513505.4667	281728.9333
Standard deviation [#/cc]	47528.4998	20576.19234
[%]	9.26%	7.30%

Table 5:Total concentrations of gold particles measured by the SMPS

	Total particle concentration before humidifier	Total particle concentration after humidifier
	[#/cc]	[#/cc]
	478502	151518
	464280	141326
	409911	138845
	503197	160174
Mean [#/cc]	4.64E+05	1.48E+05
Standard deviation [#/cc]	3.42E+04	8.50E+03
[%]	7.37%	5.74%

Table 6: Total concentrations of copper particles measured by the SMPS

	Total particle concentration before humidifier	Total particle concentration after humidifier
	[#/cc]	[#/cc]
	4.04E+06	2.21E+06
	4.73E+06	3.51E+06
	6.45E+06	3.90E+06
	4.66E+06	3.70E+06
	5.85E+06	3.08E+06
	5.01E+06	2.94E+06
	4.42E+06	2.69E+06
	4.34E+06	3.22E+06
	5.15E+06	2.81E+06
Mean [#/cc]	4.96E+06	3.12E+06
Standard deviation [#/cc]	7.23E+05	5.00E+05
[%]	14.57%	16.03%

Table 7: Total concentrations of iron particles measured by the SMPS

	Total particle concentration before humidifier	Total particle concentration after humidifier
	[#/cc]	[#/cc]
	3.43E+06	2.34E+06
	2.99E+06	2.08E+06
	2.70E+06	2.12E+06
	2.81E+06	2.12E+06
	2.77E+06	2.23E+06
	2.80E+06	1.93E+06
	3.30E+06	2.08E+06
	3.08E+06	2.03E+06
	2.77E+06	2.01E+06
Mean [#/cc]	2.96E+06	2.11E+06
Standard deviation [#/cc]	2.45E+05	1.13E+05
[%]	8.27%	5.39%

Table 8: Total concentrations of carbon particles measured by the SMPS